RT-PCR

Total RNA was isolated with RNAisoPlus reagent (Takara Bio Inc., Shiga, Japan) as specified by manufacturer. One microgram of RNA was used for the reverse transcription reactions using Superscript III First-Strand Synthesis System for RT-PCR (Invitrogen). Aliquots of cDNA were placed in a total volume of 10 μl in Platinum Blue PCR SuperMix (Invitrogen). The PCR parameters were 94°C for 15 s, 55°C for 15 s, and 72°C for 15 s, for 25 cycles (Grb2) or 30 cycles (Grb2). Five microliter of the PCR products was electrophoresed on 2% agarose gel containing SYTO60 dye (Invitrogen). The gel was scanned and analyzed with an Odyssey Infrared Imaging System (LI-COR). Primers used in this paper were as follows: glyceraldehyde-3-phosphate dehydrogenase (GAPDH), 5'-AACTTTGGCATTGTGGAGG-3' and 5'-ACACATTGGGGG-TAGGAACA-3'; Grb2, 5'-GAGCCAAGGCAGAAGAAATG-3' and 5'-CTTCACCACCCACAGGAAAT-3'.

Immunofluorescent staining

Cells were fixed with 10% formalin in PBS for 15 min, and then permeabilized with 0.5% Triton X-100. Cells were then incubated with mouse anti-sarcomeric myosin heavy chain (sMyHC) antibody (clone MF20). After washes in PBS, primary antibody binding was visualized with Alexa Fluor 488-conjugated secondary antibody (Molecular Probes, Eugene, OR) for 30 min before washing and mounting in Mowiol mounting medium containing 100 ng/ml Hoechst 33258.

Bromodeoxyuridine incorporation

C2C12 cells were fed with fresh DMEM containing 10 μM 5-bromo-2'-deoxyuridine (BrdU). After incubation for 24 h, cells were fixed with 4% paraformaldehyde in PBS, followed by permeabilization with 0.5% Triton X-100. After 2 N hydrochloric acid treatment for 10 min at room temperature, cells were immunostained for BrdU with rat anti-BrdU antibody (clone BU1/75, Abcam, Cambridge, MA) as described above. In each experiment, 5 randomly selected fields were photographed and the numbers of total and BrdU-positive nuclei were counted. Each field contained approximately 200 nuclei on the average.

Results

Quiescent satellite cells play central roles in skeletal muscle regeneration and repair. C2C12 cells, the most commonly used skeletal muscle cell line, generate quiescent satellite cell-like cells as well as differentiated myotubes (Lindon *et al.*, 1998; Yoshida *et al.*, 1998). Reserve cells are mitotically quiescent but can be activated to enter the cell cycle with FBS, judging from BrdU incorporation (Fig. 1A). Reserve cells would presumably be activated with certain growth factors, such as FGF, HGF, and IGFs, which was reported to participate in satellite cell activation (Johnson and Allen, 1995; Tatsumi *et al.*, 1998; Sheehan and Allen, 1999; Yablonka-Reuveni *et al.*, 1999; Rochat *et al.*, 2004). As shown in Fig. 1A, reserve cells were also activated with FGF2, a well-known regulator of myogenic cell proliferation (Olwin *et al.*, 1994; Sheehan and Allen, 1999; Yablonka-Reuveni *et al.*, 1999), in the presence of insulin (Fig. 1A). FGF2-induced BrdU incorporation in reserve cells was significantly suppressed with U0126, an inhibitor for MEK, suggesting the involvement of ERK1/2 in reserve cell activation induced with FGF2 (Fig. 1B).

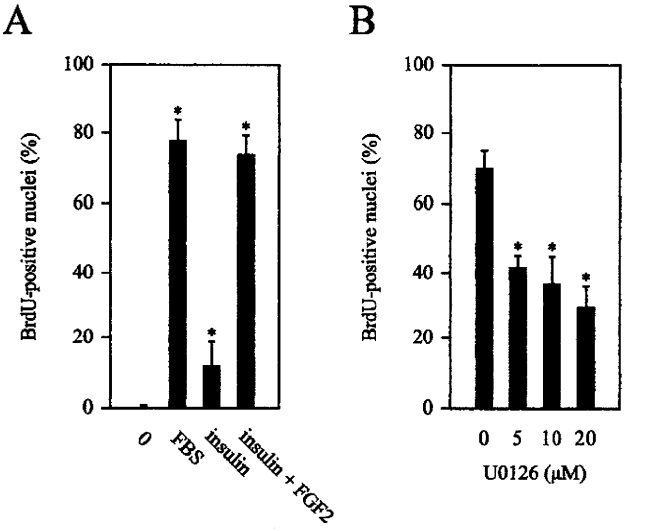

Fig. 1. FGF2-induced cell cycle entry of C2C12 reserve cells. Reserve cells were prepared by culturing C2C12 cells in serum-free differentiation medium for 5 days, and fed with BSA/DMEM containing 10 μM BrdU in the absence or presence of 10% FBS, 10 μg/ml insulin or 25 ng/ml FGF2. Cells were fixed with 10% formaldehyde after 24 h in culture, and then subjected to immunodetection of BrdU (A). After reserve cells were treated with MEK inhibitor U0126 at indicated concentrations, they were stimulated with a combination of 10 μg/ml insulin and 25 ng/ml FGF2. BrdU incorporation was examined after 24 h (B). Data presented are the mean percentage of BrdU positive nuclei±SD from three independent experiments. Asterisks indicate that data are statistically significant using a *t* test ($P<0.01$) compared to unstimulated cells (A) or U0126-untreated cells (B).

The aim of this study was to define the signaling systems responsible for the initiation and maintenance of ERK1/2 activation induced with FGF2 in reserve cells. Here, we especially focused on the PKC- and Grb2-dependent pathways by using inhibitor and/or siRNA. siRNA-mediated gene silencing was easily and reproducibly carried out in proliferating/differentiation C2C12 cells. We first tried to transfect proliferating C2C12 cells with siRNAs and confirmed efficient silencing of the target. Two independent sequences of siRNA duplexes against Grb2 (#1 and #2) were tested in this study. After cultured in serum-rich growth medium for 24 h, C2C12 cells were transfected with siRNAs in serum-free differentiation medium. At 48 h after transfection, C2C12 cells were harvested for detection of

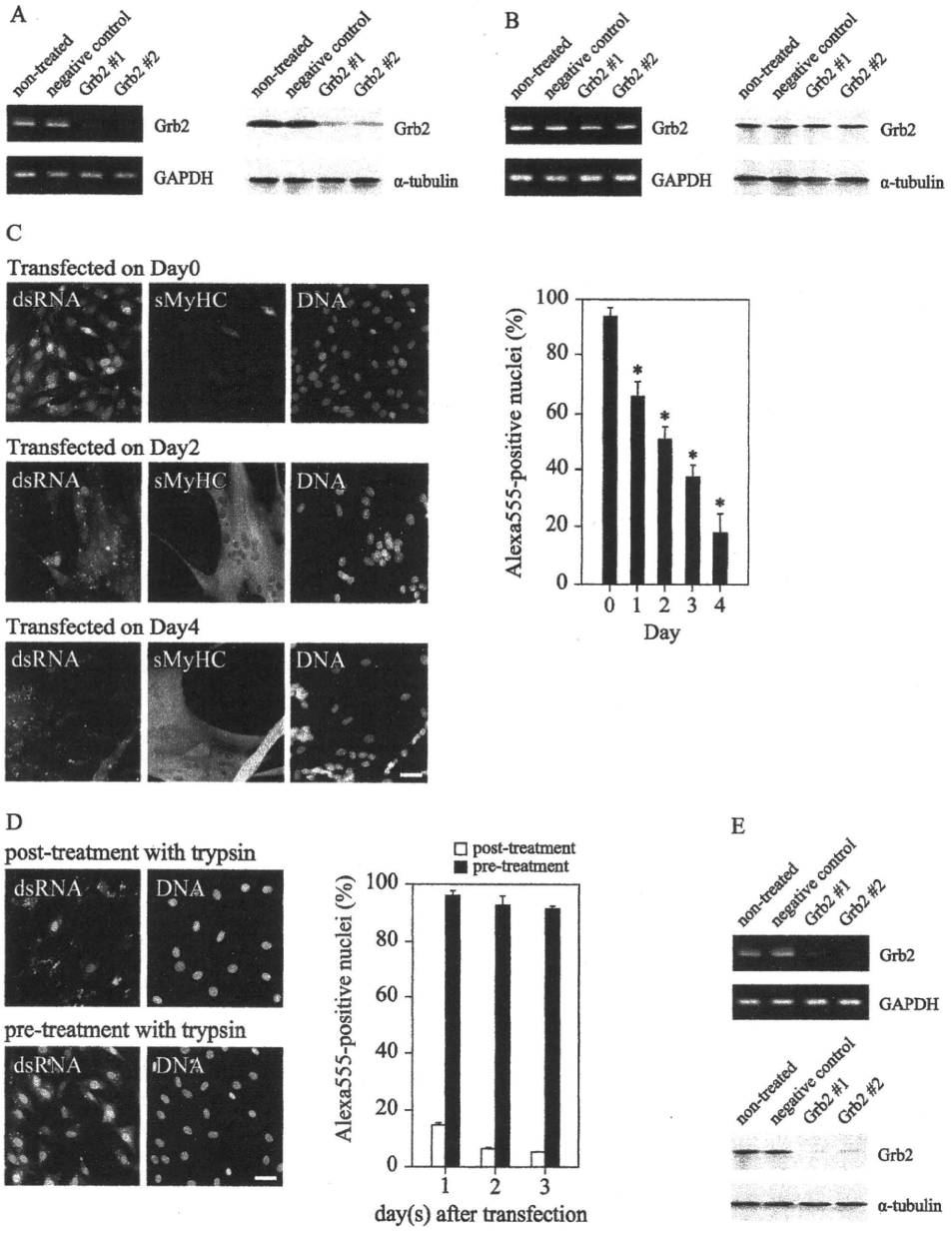

Fig. 2. Transfection of Grb2 siRNA into proliferating or quiescent C2C12 cells. (A and B) Proliferating C2C12 cells (A) or quiescent C2C12 cells cultured for 4 days in differentiation medium were transfected with siRNAs, and harvested at 2 days after the transfection for RT-PCR or Western blotting analysis. In contrast to clear decrease in Grb2 expression in proliferating cells, the effect of gene silencing was negligible. siRNAs used in experiment were negative control and 2 independent sequences for Grb2 (#1 and #2). GAPDH and α-tubulin were used as internal control for RT-PCR and Western blotting, respectively. (C) To monitor the efficiency of siRNA delivery, C2C12 cells were transfected with fluorescent labeled dsRNA at the same time or 1–4 day(s) after serum withdrawal. Cells were fixed at 24 h after transfection and immunostained for sarcomeric myosin heavy chain (sMyHC) as well as counterstained for DNA. Although transfection on Day0 resulted in efficient dsRNA delivery, the efficiency dropped significantly on Day2 and became much less on Day4. Bar: 50 μm. The percentage of red fluorescent oligo positive nuclei after the transfection was determined and represented as a graph. Bars indicate SD from three independent experiments. Asterisks indicate that data are statistically significant using a *t* test ($P<0.01$) compared to the transfection on Day0. (D) C2C12 cells cultured in differentiation medium for 4 days were transfected with fluorescent labeled dsRNA. At that time, C2C12 cells formed multinucleated myotubes and mononucleated reserve cells. Mild trypsinization detaches myotubes only, thus leaving reserve cells on culture plate. When trypsin treatment was carried out after the transfection, just before the fixation, only a few cells incorporated siRNA into their nuclei. In contrast, trypsin treatment before transfection greatly enhanced the efficiency of siRNA delivery. Bar: 50 μm. The percentage of fluorescent dsRNA oligonucleotide-positive cells treated with trypsin after transfection (blank column) and cells treated with trypsin before transfection (filled column) were represented as a graph. Bars indicate SD from three independent experiments. (E) Reserve cells were transfected with siRNAs as described above, harvested 3 days thereafter, and analyzed for Grb2 expression by RT-PCR and Western blotting. As expected, gene silencing of Grb2 was clearly observed at both mRNA- and protein-level.

Grb2 at mRNA level by RT-PCR as well as at protein level by Western blotting analysis. As shown in Fig. 2A, mRNA expression was markedly reduced with Grb2-specific siRNA. Negative control siRNA, which was designed to minimize sequence homology to any known vertebrate transcript, showed virtually no effect. Furthermore, Western blotting analysis showed Grb2 protein was effectively reduced in Grb2-specific siRNA transfected cells (Fig. 2A).

In order to define the signaling systems responsible for the initiation and maintenance of ERK1/2 activation induced with FGF2 in reserve cells, we needed to achieve efficient gene silencing in quiescent reserve cells. In contrast to successful siRNA transfection into proliferating cells (Fig. 2A), the transfection of quiescent reserve cells, which were cultured in differentiated serum-free medium for 4 days, resulted in poor silencing of Grb2 expression at both the mRNA- and protein-level (Fig. 2B).

To evaluate the efficiency of siRNA delivery into C2C12 cells, we used fluorescent-lableled double strand RNA (dsRNA) oligomer. The fluorescent dsRNA oligomer would be incorporated into cell nuclei when the transfection was achieved successfully. We examined on which day C2C12 cells can be transfected with siRNA after the induction of differentiation. C2C12 cells were induced to differentiate, and then siRNA transfections were carried out at the same time on 1–4 days thereafter with fluorescent dsRNA oligomer. Cells were fixed at 24 h after the transfection, and the uptake of fluorescent dsRNA oligomer was assessed. As shown in Fig. 2C, fluorescent signals were readily observed in nuclei when transfection was carried out at the same time of the induction of differentiation. The presence of differentiated myotubes, which expressed sMyHC, became apparent on Day2 or later (Fig. 2C). The efficiency of transfection, as well as fluorescence intensity, was severely reduced in cells cultured in differentiation medium (Fig. 2C). Only 18.1% of cells incorporated fluorescent dsRNA oligomer when transfection was carried out on Day4 (Fig. 2C). It is worth noting that aggregated fluorescence signals were frequently observed outside cells when siRNA transfection resulted in poor efficiency (Fig. 2C). We also examined how long siRNA remained after C2C12 cells were transfected with fluorescent dsRNA oligomer on Day0, and found that only 31.4% of cells possessed fluorescent signal after 5 days (data not shown). Taken together, these results suggest that the ordinary procedure does not work for transfecting quiescent reserve cells with siRNA because of severe reduction in siRNA delivery in these cells.

Mild trypsinization was reported to be useful as to obtain pure reserve cell cultures (Kitzmann *et al.*, 1998). In fact, we have also utilized the technique with some modification and established reproducible isolation (Nagata *et al.*, 2000a). Because conventional transfection did not work for siRNA transfection of reserve cells, we next tried transfection soon after reserve cell isolation. C2C12 cells were allowed to differentiate for 4 days in differentiation medium. At this time point, approximately 70% of the cells form multinucleate myotubes, while the rest of the cells remain in an undifferentiated quiescent state (Kitzmann *et al.*, 1998; Yoshida *et al.*, 1998). Cells were treated with 0.05% trypsin in PBS (+) for 5 min at 37°C. Only myotubes were detached from the cell culture plate by this treatment, while reserve cells remain attached to cell dishes. Cells were rinsed with PBS (+) to wash away detached myotubes and remaining trypsin, then fed with DMEM containing siRNA-liposome complexes. Although trypsin-treatment after the transfection did not make any improvement, nuclear-localized fluorescent signals were clearly observed in cells pre-treated with trypsin, and as a consequence, the percentage of fluorescent siRNA-positive cells was maintained at more than 90% on Day3 after transfection. (Fig. 2D)

Because fluorescent-labeled siRNA were successfully delivered into quiescent reserve cells by trypsin pretreatment, we then tried transfection with siRNAs against Grb2. Reserve cells were harvested for the analysis of the expression of Grb2 at 3 days after transfection. The decrease in mRNA expression was observed at maximum on Day3 (Fig. 2E), and concomitantly, the silencing of gene expression was also observed at protein level (Fig. 2E). Importantly, the efficient silencing of Grb2 expression in quiescent reserve cells was achieved with siRNAs at a concentration of 5 nM. There was no obvious cytotoxicity in that condition.

Since we established an efficient siRNA transfection into quiescent reserve cells, we next examined the signaling pathway of reserve cell activation. To examine the involvement of Grb2 and PKC in FGF2-induced reserve cell activation, serum-starved reserve cells were transfected with siRNA against Grb2 as described above, and then after 3 days, cells were stimulated with either FGF2 or phorbol 12-myristate 13-acetate (PMA) in the presence or absence of PKC inhibitors. Initially, reserve cells were stimulated with PMA. PMA is a well-known activator of PKC, and thus used to examine the potential role of PKC on ERK1/2 phosphorylation in reserve cells. PMA caused rapid and sustained phosphorylation of ERK1/2 (Fig. 3A), suggesting the presence of a PKC-mediated pathway leading to ERK phosphorylation in reserve cells.

We used a combination of two PKC inhibitors, namely, Gö6976 (Martiny-Baron *et al.*, 1993) and Gö6983 (Gschwendt *et al.*, 1996), to inhibit almost all isoforms of PKC as reported (Shu *et al.*, 2002). After 30 min pretreatment with PKC inhibitors, reserve cells were stimulated with PMA for 15 min and then harvested for Western blotting analysis. In reserve cells, the combination of Gö6976 and Gö6983 almost completely suppressed PMA-induced phosphorylation of ERK1/2 (Fig. 3B). Although expression levels of Grb2 were reproducibly decreased to less than 10% of normal level in Grb2-siRNA treated cells, the silencing of Grb2 did not have any effect on ERK phosphorylation in PMA-stimulated reserve cells (Fig. 3B),

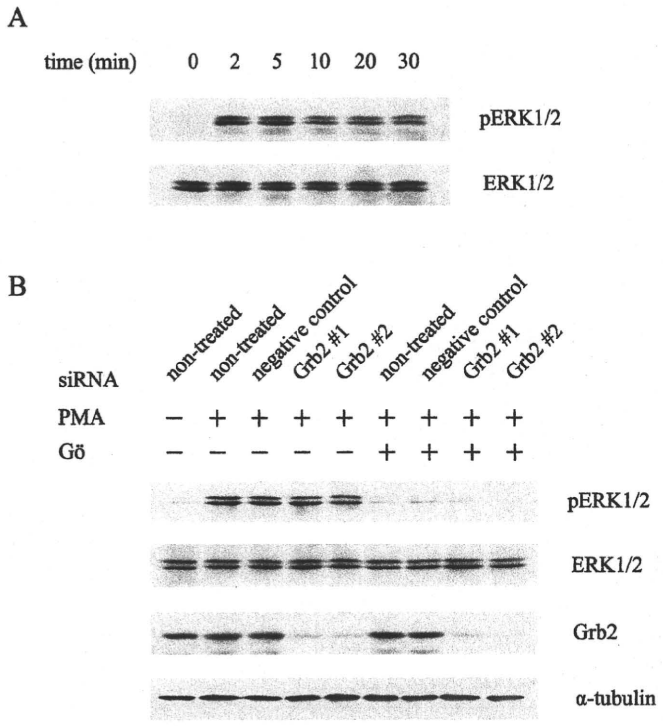

Fig. 3. Analysis of PKC- and Grb2-dependent ERK phosphorylation in PMA-stimulated reserve cells. (A) Serum-starved reserve cells were transfected with siRNA against Grb2 after pretreatment with trypsin, and then 3 days later, cells were fed with 100 nM PMA. After incubation for 2–30 min, cells were harvested for the analysis of ERK phosphorylation. (B) Before PMA was added, reserve cells transfected with siRNAs were treated with a combination of two PKC inhibitors, 1 μM Gö6976 and 1 μM Gö6983. Fifteen minutes after PMA stimulation, cells were harvested for Western blotting analysis. Expression levels of phospho-ERK1/2, ERK1/2, Grb2, α-tubulin were detected with their specific antibodies.

demonstrating that PKC phosphorylated ERK independent of Grb2.

PKC has been reported to mediate peptide growth factor induced signaling pathways (Presta *et al.*, 1989; Nishizuka, 1992; Kim *et al.*, 2003; Clerk *et al.*, 2006).

Indeed, FGF2, as well as PMA, caused phosphorylation of PKC especially with higher molecular weight (Fig. 4A). The PKC antibody used in this study recognizes α, βI, βII, δ, ε, η, and θ isoforms only when phosphorylated at an autophosphorylation site (Keranen *et al.*, 1995). The similar band patterns were reported previously (Sweeney *et al.*, 2001).

FGF2 caused robust and transient phosphorylation of ERK1/2 in reserve cells, detectable within 2 min after the stimulation, peaked around 5 min (Fig. 4B). The suppression of ERK phosphorylation by PKC inhibition was prominent at 2 min. Interestingly, higher levels of phosphorylated ERK1/2 were detected at later time points in Gö-treated cells compared to untreated cells (Fig. 4B). Gene-silencing of Grb2 resulted in decreased levels of ERK phosphorylation at any time point, but certain levels of phosphorylated ERK1/2 were detectable (Fig. 4B).

For close examination of FGF2-induced ERK phosphorylation, cells were treated with the combination of siRNA and PKC inhibitors, and then sampled at 2, 15, and 30 min after FGF2 stimulation. At 2 min after FGF2 stimulation, phosphorylation of ERK1/2 was significantly suppressed with either siRNA against Grb2 or PKC inhibitors. Almost complete suppression of ERK phosphorylation was observed when cells were transfected with Grb2-specific siRNA followed by treatment with PKC inhibitors (Fig. 4C). Although ERK phosphorylation which was dependent on Grb2 still existed at high levels, sensitivity of PKC inhibition was not observed at 15 min (Fig. 4C). Only weak signals of phosphorylated ERK1/2 were detectable at 30 min in normal conditions, but PKC-inhibition resulted in higher levels of ERK phosphorylation (Fig. 4C), suggesting the presence of PKC-mediated suppression of receptor-coupled tyrosine kinase activity (Cochet *et al.*, 1984) at later time points. Notably, as shown in Fig. 4C, phosphorylation of ERK1/2 at 30 min was dependent on Grb2, in contrast to PMA-induced ERK phosphorylation (see Fig. 3B).

Collectively, these results demonstrated that FGF2 induced phosphorylation of ERK1/2 in a manner dependent on both Grb2 adapter protein and PKC with distinct kinetics.

Discussion

Quiescent satellite cells must be initially activated before participating in skeletal muscle regeneration and repair. Although it is widely known that certain stimuli, such as injury, overload, and exercise, cause activation of satellite cells (reviewed in Charge and Rudnicki, 2004), the molecular mechanisms in the control of satellite cell activation is largely unknown. FGF2 is an established mitogen for myogenic cells and implicated in satellite cell activation (Olwin *et al.*, 1994; Sheehan and Allen, 1999; Yablonka-Reuveni *et al.*, 1999). We showed FGF2 made reserve cells enter the cell cycle partially through the ERK pathway. ERK plays an important role in the control of various cellular responses, including cell proliferation, differentiation, and survival. A variety of growth factors and cytokines are known to activate ERK1/2 via a complicated signaling network. In addition to the Grb2/Sos-mediated pathway, other distinct signaling cascades such as a PLC/PKC- or a PI3K/Akt-mediated pathway could also contribute to ERK activation (reviewed in Schlessinger, 2000).

We showed FGF2 induced phosphorylation of ERK1/2 was mostly dependent on both Grb2 and PKC because ERK phosphorylation was almost, if not completely, suppressed by a combined treatment with Grb2-specific siRNA and PKC inhibitors. Therefore, delayed and sustained phosphorylation of ERK in the presence of PKC inhibitors would reflect mostly the Grb2-mediated pathway. Higher levels of

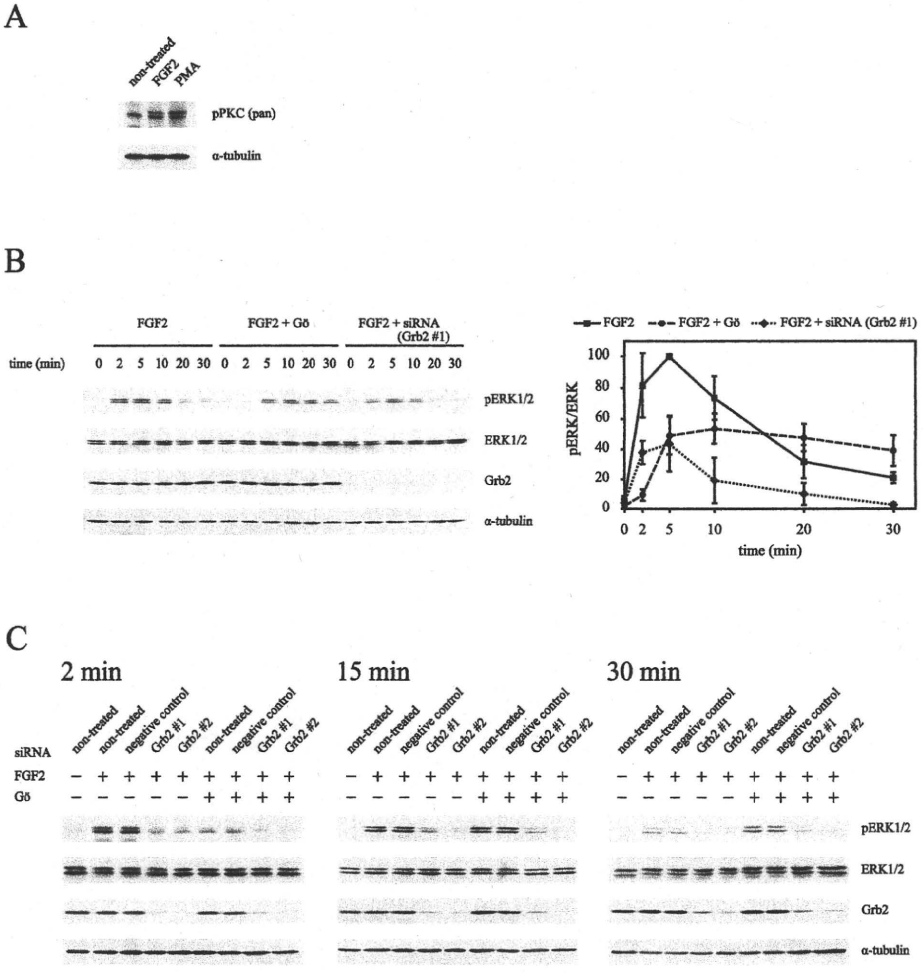

Fig. 4. Analysis of PKC- and Grb2-dependent ERK phosphorylation in FGF2-stimulated reserve cells. (A) Reserve cells were incubated with either FGF2 for 5 min or PMA for 15 min, and then harvested for the analysis of PKC phosphorylation by Western blotting. The PKC antibody used in this study recognizes α, βI, βII, δ, ε, η, and θ isoforms only when phosphorylated at an autophosphorylation site. (B) FGF2-induced ERK phosphorylation was examined in reserve cells which were in normal condition, treated with PKC inhibitors, or transfected with siRNA against Grb2 (#1). At 2–30 min after stimulation, cells were harvested for the analysis of ERK phosphorylation. The intensities of phosphor-ERK/ERK were measured and normalized to the value of phosphor-ERK/ERK at 5 min in FGF2-stimulated reserve cells in normal conditions. Bars indicate SD from three independent experiments. (C) Reserve cells transfected with siRNAs were treated with a combination of PKC inhibitors, and then fed with FGF2. Cells were harvested for Western blotting analysis at 2, 15 or 30 min after the stimulation. Expression levels of phospho-ERK1/2, ERK1/2, Grb2, and α-tubulin were detected with their specific antibodies.

ERK phosphorylation at later time points would demonstrate PKC-mediated suppression of receptor-coupled tyrosine kinase activity (Cochet *et al.*, 1984) in normal conditions. On the other hand, rapid phosphorylation of ERK observed in cells transfected with Grb2 specific siRNAs would mostly demonstrate the PKC-mediated pathway. Taken together, we would conclude that FGF2-caused ERK phosphorylation is dependent on both the Grb2- and the PKC-mediated pathway, and that the PKC-mediated pathway contributes to rapid initiation and termination of ERK phosphorylation, while the Grb2-mediated pathway contributes to delayed and sustained ERK phosphorylation.

In this study, we achieved efficient siRNA transfection of quiescent reserve cells. For siRNA transfection, exponentially growing cells are preferentially used (Elbashir *et al.*, 2002). In fact, we showed that inefficient knockdown of Grb2 expression occurred in quiescent reserve cells by common transfection protocol (Fig. 2B). That is because of poor delivery of siRNA into nuclei as the delivery of fluorescent labeled siRNA was significantly reduced after cells were induced to differentiation by serum withdrawal. Surprisingly though, remarkable improvement of siRNA delivery was observed when transfection was carried out after mild trypsinization. Furthermore, knockdown of Grb2 expression has also occurred efficiently in the trypsin-treated cells before transfection. Several studies have reported siRNA-

mediated gene silencing in quiescent cells or other cell types by transfection of proliferating cells with siRNAs followed by making cells quiescent by serum withdrawal (Asano *et al.*, 2005; Tullai *et al.*, 2007). However, this protocol was unsuitable for a loss-of-function analysis of Grb2 in reserve cells since the absence of Grb2 in proliferating C2C12 cells resulted in significant loss of reserve cells (data not shown). Because reserve cells are prepared by serum withdrawal, which causes apoptosis as well as differentiation, it is predicted that the suppression of gene products which control cell proliferation, differentiation, or apoptosis would cause abnormalities in the formation of reserve cells. In contrast, our technique had much less effect on reserve cell formation, thus enabling reliable loss-of-function analyses in reserve cells. It was shown that efficient knockdown was carried out in quiescent human bladder carcinoma cells without extra manipulation except that they used 50 nM of siRNA, five times higher concentrations than normally used, which caused significantly more cell death possibly because of off-target effect (Nabatiyan and Krude, 2004). On the other hand, our method does not require high concentration of siRNA and apparent cytotoxicity was not observed. Because aggregated fluorescent signals were observed only when siRNA transfection resulted in poor efficiency, we conjectured that siRNA/liposome complexes are trapped extracellularly in such conditions. We also speculated trypsin-treatment removed sticky molecules existing in the differentiated cell culture, which thus made siRNA/liposome complexes accessible to reserve cells. We have previously shown that the expression level of sphingomyelin was decreased as satellite cells were activated (Nagata *et al.*, 2006a), and that sphingosine-1-phosphate, one of sphingomyelin metabolites, contributed to the transition of satellite cells from quiescent to proliferative (Nagata *et al.*, 2006b). Detailed analysis of signaling pathways in the activation of reserve cells, as a model of satellite cells, would become possible by applying siRNA-mediated gene silencing in quiescent reserve cells.

In this study, we revealed that FGF2 caused ERK phosphorylation in a manner dependent on both Grb2 and PKC with different kinetics by efficient gene silencing of Grb2 in quiescent reserve cells. Successful gene silencing in reserve cells would be applicable to other gene products, thus would be useful to examine the molecular mechanisms in the activation of quiescent satellite cells as well as in the maintenance of quiescent state.

Acknowledgments. We would like to thank Dr. P.S. Zammit (King's College London) for critical reading of the manuscript. This research was supported by the MEXT (The Ministry of Education, Culture, Sports, Science and Technology) (Grant-in-Aid for Young Scientists (B), 19770189), Japan. This research was also partially supported by grants 18A-1 for Nervous and Mental Disorders and H19-kokoro-020 for Research in Brain Science from MHLW (The Ministry of Health, Labour and Welfare), Japan, and grants 17570058 and 14654174 from MEXT, Japan.

References

Asano, T., Yao, Y., Shin, S., McCubrey, J., Abbruzzese, J.L., and Reddy, S.A. 2005. Insulin receptor substrate is a mediator of phosphoinositide 3-kinase activation in quiescent pancreatic cancer cells. *Cancer Res.*, **65**: 9164–9168.

Blau, H.M., Chiu, C.P., and Webster, C. 1983. Cytoplasmic activation of human nuclear genes in stable heterocaryons. *Cell*, **32**: 1171–1180.

Charge, S.B. and Rudnicki, M.A. 2004. Cellular and Molecular Regulation of Muscle Regeneration. *Physiol. Rev.*, **84**: 209–238.

Clerk, A., Aggeli, I.K., Stathopoulou, K., and Sugden, P.H. 2006. Peptide growth factors signal differentially through protein kinase C to extracellular signal-regulated kinases in neonatal cardiomyocytes. *Cell. Signal.*, **18**: 225–235.

Cochet, C., Gill, G.N., Meisenhelder, J., Cooper, J.A., and Hunter, T. 1984. C-kinase phosphorylates the epidermal growth factor receptor and reduces its epidermal growth factor-stimulated tyrosine protein kinase activity. *J. Biol. Chem.*, **259**: 2553–2558.

Elbashir, S.M., Harborth, J., Weber, K., and Tuschl, T. 2002. Analysis of gene function in somatic mammalian cells using small interfering RNAs. *Methods*, **26**: 199–213.

Grammer, T.C. and Blenis, J. 1997. Evidence for MEK-independent pathways regulating the prolonged activation of the ERK-MAP kinases. *Oncogene*, **14**: 1635–1642.

Gschwendt, M., Dieterich, S., Rennecke, J., Kittstein, W., Mueller, H.J., and Johannes, F.J. 1996. Inhibition of protein kinase C mu by various inhibitors. Differentiation from protein kinase c isoenzymes. *FEBS Lett.*, **392**: 77–80.

Johnson, S.E. and Allen, R.E. 1995. Activation of skeletal muscle satellite cells and the role of fibroblast growth factor receptors. *Exp. Cell Res.*, **219**: 449–453.

Keranen, L.M., Dutil, E.M., and Newton, A.C. 1995. Protein kinase C is regulated in vivo by three functionally distinct phosphorylations. *Curr. Biol.*, **5**: 1394–1403.

Kim, H.J., Kim, J.H., Bae, S.C., Choi, J.Y., and Ryoo, H.M. 2003. The protein kinase C pathway plays a central role in the fibroblast growth factor-stimulated expression and transactivation activity of Runx2. *J. Biol. Chem.*, **278**: 319–326.

Kitzmann, M., Carnac, G., Vandromme, M., Primig, M., Lamb, N.J., and Fernandez, A. 1998. The muscle regulatory factors MyoD and myf-5 undergo distinct cell cycle-specific expression in muscle cells. *J. Cell Biol.*, **142**: 1447–1459.

Kouhara, H., Hadari, Y.R., Spivak-Kroizman, T., Schilling, J., Bar-Sagi, D., Lax, I., and Schlessinger, J. 1997. A lipid-anchored Grb2-binding protein that links FGF-receptor activation to the Ras/MAPK signaling pathway. *Cell*, **89**: 693–702.

Lindon, C., Montarras, D., and Pinset, C. 1998. Cell cycle-regulated expression of the muscle determination factor Myf5 in proliferating myoblasts. *J. Cell Biol.*, **140**: 111–118.

Margolis, B. 1999. The PTB Domain: The Name Doesn't Say It All. *Trends Endocrinol. Metab.*, **10**: 262–267.

Martiny-Baron, G., Kazanietz, M.G., Mischak, H., Blumberg, P.M., Kochs, G., Hug, H., Marme, D., and Schachtele, C. 1993. Selective inhibition of protein kinase C isozymes by the indolocarbazole Go 6976. *J. Biol. Chem.*, **268**: 9194–9197.

Mauro, A. 1961. Satellite cells of skeletal muscle fibres. *J. Biophys. Bipchem. Cytol.*, **9**: 493–495.

Nabatiyan, A. and Krude, T. 2004. Silencing of chromatin assembly factor 1 in human cells leads to cell death and loss of chromatin assembly during DNA synthesis. *Mol. Cell. Biol.*, **24**: 2853–2862.

Nagata, Y., Kobayashi, H., Umeda, M., Ohta, N., Kawashima, S., Zammit, P.S., and Matsuda, R. 2006a. Sphingomyelin levels in the plasma membrane correlate with the activation state of muscle satellite cells. *J. Histochem. Cytochem.*, **54**: 375–384.

Nagata, Y., Partridge, T.A., Matsuda, R., and Zammit, P.S. 2006. Entry of muscle satellite cells into the cell cycle requires sphingolipid signaling. *J. Cell Biol.*, **174**: 245–253.

Nishizuka, Y. 1992. Intracellular signaling by hydrolysis of phospholipids and activation of protein kinase C. *Science*, **258**: 607–614.

Olwin, B.B., Hannon, K., and Kudla, A.J. 1994. Are fibroblast growth factors regulators of myogenesis in vivo? *Prog. Growth Factor Res.*, **5**: 145–158.

Presta, M., Maier, J.A., and Ragnotti, G. 1989. The mitogenic signaling pathway but not the plasminogen activator-inducing pathway of basic fibroblast growth factor is mediated through protein kinase C in fetal bovine aortic endothelial cells. *J. Cell Biol.*, **109**: 1877–1884.

Rochat, A., Fernandez, A., Vandromme, M., Moles, J.P., Bouschet, T., Carnac, G., and Lamb, N.J. 2004. Insulin and wnt1 pathways cooperate to induce reserve cell activation in differentiation and myotube hypertrophy. *Mol. Biol. Cell*, **15**: 4544–4555.

Schlessinger, J. 2000. Cell signaling by receptor tyrosine kinases. *Cell*, **103**: 211–225.

Sheehan, S.M. and Allen, R.E. 1999. Skeletal muscle satellite cell proliferation in response to members of the fibroblast growth factor family and hepatocyte growth factor. *J. Cell. Physiol.*, **181**: 499–506.

Shu, X., Wu, W., Mosteller, R.D., and Broek, D. 2002. Sphingosine kinase mediates vascular endothelial growth factor-induced activation of ras and mitogen-activated protein kinases. *Mol. Cell. Biol.*, **22**: 7758–7768.

Sun, X.J., Crimmins, D.L., Myers, M.G., Jr., Miralpeix, M., and White, M.F. 1993. Pleiotropic insulin signals are engaged by multisite phosphorylation of IRS-1. *Mol. Cell. Biol.*, **13**: 7418–7428.

Sweeney, C., Pambrough, D., Huard, C., Diamond, A.J., Lander, E.S., Cantley, L.C., and Carraway, K.L., 3rd 2001. Growth factor-specific signaling pathway stimulation and gene expression mediated by ErbB receptors. *J. Biol. Chem.*, **276**: 22685–22698.

Tatsumi, R., Anderson, J.E., Nevoret, C.J., Halevy, O., and Allen, R.E. 1998. HGF/SF is present in normal adult skeletal muscle and is capable of activating satellite cells. *Dev. Biol.*, **194**: 114–128.

Tullai, J.W., Chen, J., Schaffer, M.E., Kamenetsky, E., Kasif, S., and Cooper, G.M. 2007. Glycogen synthase kinase-3 represses cyclic AMP response element-binding protein (CREB)-targeted immediate early genes in quiescent cells. *J. Biol. Chem.*, **282**: 9482–9491.

Yablonka-Reuveni, Z., Seger, R., and Rivera, A.J. 1999. Fibroblast growth factor promotes recruitment of skeletal muscle satellite cells in young and old rats. *J. Histochem. Cytochem.*, **47**: 23–42.

Yaffe, D. and Saxel, O. 1977. Serial passaging and differentiation of myogenic cells isolated from dystrophic mouse muscle. *Nature*, **270**: 725–727.

Yoshida, N., Yoshida, S., Koishi, K., Masuda, K., and Nabeshima, Y. 1998. Cell heterogeneity upon myogenic differentiation: down-regulation of MyoD and Myf-5 generates 'reserve cells'. *J. Cell Sci.*, **111**: 769–779.

Zammit, P.S., Partridge, T.A., and Yablonka-Reuveni, Z. 2006. The skeletal muscle satellite cell: the stem cell that came in from the cold. *J. Histochem. Cytochem.*, **54**: 1177–1191.

(Received for publication, November 6, 2009, accepted, April 22, 2010 and published online, May 1, 2010)

Mol Cell Biochem (2011) 350:1–11
DOI 10.1007/s11010-010-0677-1

Mitochondrial adaptations in skeletal muscle to hindlimb unloading

Akira Wagatsuma · Naoki Kotake · Takayuki Kawachi · Masataka Shiozuka · Shigeru Yamada · Ryoichi Matsuda

Received: 17 June 2010 / Accepted: 2 December 2010 / Published online: 17 December 2010

Abstract To gain insight into the regulation of mitochondrial adaptations to hindlimb unloading (HU), the activity of mitochondrial enzymes and the expression of nuclear-encoded genes which control mitochondrial properties in mouse gastrocnemius muscle were investigated. Biochemical and enzyme histochemical analysis showed that subsarcolemmal mitochondria were lost largely than intermyofibrillar mitochondria after HU. Gene expression analysis revealed disturbed or diminished gene expression patterns. The three main results of this analysis are as follows. First, in contrast to peroxisome proliferator-activated receptor γ coactivator 1 β (PGC-1β) and PGC-1-related coactivator, which were down-regulated by HU, PGC-1α was up-regulated concomitant with decreased expression of its DNA binding transcription factors, PPARα, and estrogen-related receptor α (ERRα). Moreover, there was no alteration in expression of nuclear respiratory factor 1, but its down-stream target gene, mitochondrial transcription factor A, was down-regulated. Second, both mitofusin 2 and fission 1, which control mitochondrial morphology, were down-regulated. Third, ATP-dependent Lon protease, which participates in mitochondrial-protein degradation, was also down-regulated. These findings suggest that HU may induce uncoordinated expression of PGC-1 family coactivators and DNA binding transcription factors, resulting in reducing ability of mitochondrial biogenesis. Furthermore, down-regulation of mitochondrial morphology-related genes associated with HU may be also involved in alterations in intracellular mitochondrial distribution.

Keywords Adaptation · Atrophy · Hindlimb unloading · Mitochondria · Skeletal muscle

A. Wagatsuma (✉) · T. Kawachi · M. Shiozuka · S. Yamada · R. Matsuda
Department of Life Sciences, Graduate School of Arts and Sciences, The University of Tokyo, 3-8-1 Komaba, Meguro-ku, Tokyo, Japan
e-mail: wagatsuma1969@yahoo.co.jp

N. Kotake
Department of Advanced Interdisciplinary Studies (AIS), Graduate School of Engineering, The University of Tokyo, 4-6-1 Komaba, Meguro-ku, Tokyo, Japan

Introduction

Mitochondria play important roles in energy homeostasis, metabolism, signaling, and apoptosis [1]. The abundance, morphology, and functional properties of mitochondria are dynamically regulated in response to alterations in neuromuscular activity. Basically, physical activity (e.g., exercise, endurance training, and interval training) promotes mitochondrial biogenesis, [2] whereas disuse (e.g., denervation, immobilization, spaceflight, and hindlimb unloading) discourages mitochondrial biogenesis [3–5].

A model of hindlimb unloading (HU) of a rodent is frequently used to simulate and study neuromuscular perturbations occurring in a real microgravity environment during spaceflights [6]. This earth-based model of microgravity is characterized by reduction of motor activity and lack of load bearing [7]. The major modifications concerning HU are muscle atrophy [4] and slow-to-fast fiber-type switching [7]. In addition, experimental evidence for mitochondrial adaptations to HU is accumulating; for example, mitochondrial fragmentation [8], decreased mitochondrial enzyme activity [9–14], and reduced mitochondrial oxygen consumption [9] have been reported. However, these adaptive mechanisms concerning HU remain to be elucidated. Understanding these adaptive

mechanisms may extend our knowledge of skeletal muscle plasticity and provide important insights into both space-flight- and earth-based health problems.

The adaptive mechanisms may be associated with transcriptional alterations in expression of mitochondrial biogenesis-related and other mitochondria-related genes. Mitochondrial biogenesis is a complex biological process that requires the system to import and incorporate proteins and lipids into the existing mitochondrial reticulum as well as to replicate mitochondrial DNA (mtDNA) [1]. The transcriptional mechanism that controls mitochondrial biogenesis is a complex network. The peroxisome proliferator-activated receptor, γ, coactivator 1 (PGC-1) family of transcriptional coactivators interact with multiple DNA binding transcription factors to coordinate the regulation of multiple mitochondrial genes [1]. PGC-1α coactivates expression of estrogen-related receptor α (ERRα), which activates expression of peroxisome proliferator-activated receptor α (PPARα), nuclear respiratory factor 1 (NRF-1), and NRF-2 [15]. NRF-1 activates expression of oxidative phosphorylation components, mitochondrial transporters, and mitochondrial ribosomal proteins [1]. In addition, NRF-1 regulates expression of mitochondrial transcription factor A (TFAM), contributing to mtDNA replication and transcription [16]. Apart from mitochondrial biogenesis, a recent report has highlighted the importance of mitochondrial dynamics in cell and animal physiology. Mitochondria constantly fuse and divide, and an imbalance of these two processes dramatically alters overall mitochondrial morphology and function [17]. Mitochondrial fission is driven by dynamin 1-like and fission 1, while mitochondrial fusion is controlled by mitofusins and OPA 1 [18]. Moreover, ATP-dependent Lon protease is known to catalyze the degradation of oxidatively modified matrix proteins [19]. These nuclear-encoded genes which control mitochondrial properties may therefore be key contributors to mitochondrial adaptations to HU.

In this study, we hypothesize that mitochondrial adaptations to HU are due, at least in part, to transcriptional alterations in expression of nuclear-encoded genes which control mitochondrial properties. To test this hypothesis, we investigated the activity of mitochondrial enzymes and the expression of nuclear-encoded genes involved in mitochondrial biogenesis, mitochondrial morphogenesis, and mitochondrial-protein degradation in mouse gastrocnemius muscle.

Materials and methods

Animals

Female seven-week-old CD1 mice (Clea Japan, Meguro, Tokyo) were used and housed in the animal care facility under a 12-h light/12-h dark cycle at room temperature (23 ± 2°C) and 55 ± 5% humidity. Mice were matched by body weight and then assigned to one of two groups as follows: ground-based control ($n = 12$) or HU ($n = 12$). The mice were procured after approval for this study from The University of Tokyo Animal Ethics Committee.

Preparation of mitochondria population

Two mitochondrial fractions, termed subsarcolemmal (SS) and intermyofibrillar (IMF) mitochondria, were isolated from skeletal muscle as previously reported [20]. Briefly, the skeletal muscle (the deep-red region of the gastrocnemius) was removed and immediately placed in ice-cold isolation buffer (IB). The muscles were freed of fat and connective tissue, transferred into fresh IB, and weighed. All further procedures were carried out at 0–5°C. The muscle sample was next minced with triple scissors in IB. The muscle sample was homogenized by using a tissue homogenizer for 10 s. The homogenate was centrifuged at 800*g* for 10 min, and the resulting precipitate was subsequently used for the preparation of the IMF mitochondria. The final SS mitochondrial pellet was suspended in IB. The pellet from the 800*g* centrifugation contained primarily intact material with some remaining SS mitochondria. This pellet was then washed, and the IMF mitochondria were liberated with nagarse incubation. After two washes were performed, the final IMF mitochondrial pellet was suspended in IB. The final mitochondrial protein concentration was determined by a micro bicinchoninic acid (BCA) assay (Pierce Chemical Co., Rockford, IL) with bovine serum albumin as a standard.

Procedure for hindlimb unweighting

A rat-hindlimb-suspension model, originally described in [21], was modified for use with mice [22]. Briefly, each mouse was weighed and anesthetized with an intraperitoneal injection of pentobarbital (50 mg/kg body weight). We wrapped bandages (Nichiban, Bunkyo, Tokyo) around the tail of the mice. After the mouse had recovered from the anesthetic, a swivel hook was placed through the bandage distal to the tip of the tail. This method allows the animals full 360° rotation as well as access to food and water without allowing the hindlimbs to contact the cage floor or walls. HU was continued for 7 days. All the procedures in the animal experiments were carried out in accordance with the guidelines presented in the Guiding Principles for the Care and Use of Animals in the Field of Physiological Sciences, published by the Physiological Society of Japan.

Enzyme activity assay

The activity of citrate synthase (CS) was determined spectrophotometrically according to Srere [23]. Briefly, skeletal muscle (the deep-red region of the gastrocnemius) was homogenized in 175 mM KCl, 10 mM GSH, and 2 mM EDTA at pH 7.4. The homogenate thus obtained was frozen and thawed four times and mixed thoroughly before enzymatic measurements were performed. The principle of the assay is to initiate the reaction of acetyl-CoA with oxaloacetate and the link the release of free CoA-SH to a colorimetric reagent, 5,5-dithiobis-(2-nitrobenzoate) (DTNB). The absorbance of the reaction mixtures was monitored at wavelength of 405 nm at 15 s intervals for a period of 3 min. The activity of 3-hydroxyacyl-CoA dehydrogenase (3-HAD) was assayed by measuring the decrease in absorbance at 340 nm due to the oxidation of NADH in the presence of acetoacetyl-CoA as described [24]. The absorbance of the reaction mixtures was monitored at 15 s intervals for a period of 5 min. The enzyme activities were normalized in regard to wet weight of skeletal muscle.

Enzyme histochemical analysis

To examine mitochondrial location in a myofiber, succinate dehydrogenase (SDH) staining was carried out according to Nachlas et al. [25] with minor modification. Briefly, frozen transverse sections from the mid-belly region of the gastrocnemius muscles were incubated for 10 min at 37°C in a medium (0.9 mM 1-methoxyphenazine methylsulfate, 1.5 mM nitro blue tetrazolium, 5.6 mM EDTA, and 48 mM succinate disodium salt at pH 7.6) in a 0.1 M phosphate buffer, rinsed for 5 min with deionized H_2O, dehydrated for 5 min within a myofiber in 50% acetone, and then air-dried. The fiber cross-sectional area (FCSA) and length of SDH activity wit were measured by using ImageJ software (ver. 1.42, http://rsb.info.nih.gov/ij/).

Gene expression analysis

Total RNA was prepared with TRI reagent (Molecular Research Center, Cincinnati, OH). The DNase-treated total RNA was converted to cDNA by using a first-strand cDNA synthesis system for quantitative RT-PCR (Marligen, Biosciences, Ijamsville, MD). The cDNA samples were aliquoted and stored at −80°C. Real-time PCR was carried out using an Opticon™ DNA engine (MJ Research, Waltham, MA) according to the manufacturer's instructions. The reactions employed gene-specific primers for citrate synthase, mitofusin 2, fission1, Lon protease (Takara Bio Inc., Otsu, Shiga), succinate dehydrogenase [26], medium-chain acyl-coenzyme A dehydrogenase (MCAD) [27], peroxisome proliferator-activated receptor, γ, coactivator 1α (PGC-1α), peroxisome proliferator-activated receptor, γ, coactivator 1β (PGC-1β) [28], peroxisome proliferator-activated receptor, γ, coactivator-related 1 (PRC), PPARα [29], mitochondrial transcription factor A (TFAM), mitochondrial single-stranded DNA binding protein 1 (mtSSB) [30], NRF-1, NRF-2 [31], ERRα [32], and manganese superoxide dismutase (MnSOD) [33]. PCR thermal-cycle conditions were optimized to achieve a single ethidium bromide-stained band following electrophoresis on a 2% agarose gel. Differences in gene expression were calculated relative to the expression of a housekeeping gene by comparison with a standard curve. To identify the appropriate housekeeping gene, we investigated several housekeeping genes including 18S ribosomal RNA, glyceraldehyde-3-phosphate dehydrogenase, β-actin, and cyclophilin. We selected cyclophilin as the housekeeping gene because its expression levels remain unchanged in hindlimb-unloaded muscle relative to control muscle. Cyclophilin was found to be appropriate for normalizing the signal by comparing the differences in raw threshold cycle values (i.e., the number of amplification cycles at which the signal is detected above the background and is in the exponential phase). A standard curve was constructed from serially diluted cDNA of gastrocnemius muscle. Each sample was normalized by its cyclophilin content. The final results were expressed as a relative fold change compared to that of control animals.

Statistics

Data are means ± SEM. For analysis between the control and HU cases, Student's t test was used to determine significance. The level of significance was set at $P < 0.05$.

Results

To assess whether the mouse model mimics the rat model previously reported, the degree of muscle atrophy was estimated, and the expression of atrogin-1 mRNA, muscle-specific ubiquitin-ligase, which is known to mediate rodent muscle atrophy, was investigated. Myofibers from hindlimb-unloaded mice were pathologically atrophied in reference to those from control mice. Significant decreases in the FCSA of two types of myofiber (52% for SDH^{High} and 51% for SDH^{Low}) were observed after 7 days of HU. Moreover, atrogin-1 mRNA transcript was strongly induced in the HU case compared to the control case (Fig. 1).

Subsarcolemmal mitochondria were degraded more rapidly than IMF mitochondria during HU [8]. Therefore, we isolated SS and IMF mitochondria from control and hindlimb-unloaded mice. As expected, SS mitochondria

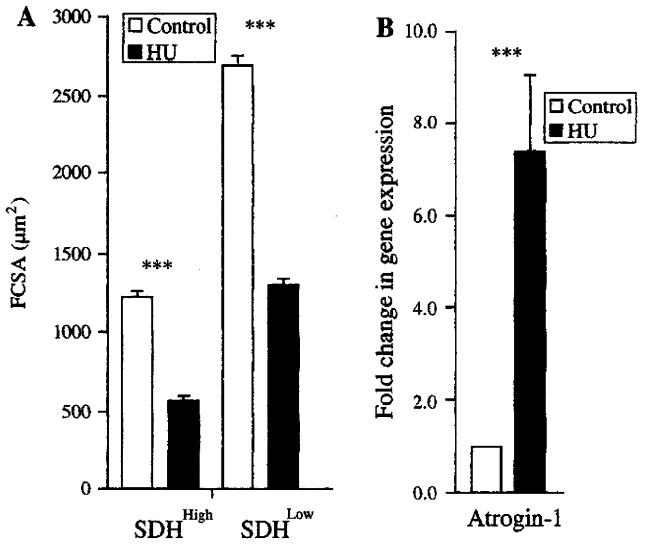

Fig. 1 Effects of HU on myofiber size and mRNA expression levels of atrogin-1, a muscle-specific ubiquitin-ligase required for muscle atrophy. **a** After 7 days of HU, muscle tissues were cryosectioned and reacted for SDH activity. Myofibers were divided into two groups: SDH^{High} (dark stain) and SDH^{Low} (light stain). FCSA was measured with the image-analysis system, calibrated to transform the number of pixels (viewed on a computer monitor) into micrometers. **b** To investigate mRNA expression levels between control and HU, total RNA was isolated from muscle tissues and relative gene expression was quantified by real-time PCR. Cyclophilin was used internal control. The data are means ± SEM ($n = 6$). Statistically significant differences compared to control: $^{***}P < 0.001$

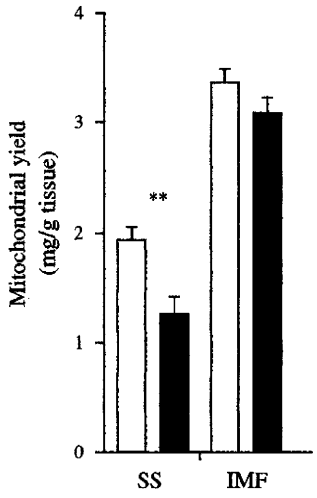

Fig. 2 Effects of HU on quantitative alteration in mitochondria in SS and IMF regions of muscle fibers. SS and IMF mitochondrial fractions were isolated from control and hindlimb-unloaded mice by differential centrifugation and digestion techniques. Mitochondrial protein content was determined using micro BCA assay and the yield was expressed as mg/g tissue weight. The data are means ± SEM ($n = 6$). Statistically significant differences compared to control: $^{**}P < 0.01$

were significantly decreased in the HU case compared to that in the control case. Although IMF mitochondria also showed a tendency to decrease after HU, there was no significant difference between groups (Fig. 2).

Because HU decreases the activity of mitochondrial enzymes, the activity of CS was measured. The activity was significantly decreased in the HU case compared to that in the control case. It has been reported that HU suppressed gene expression of enzyme in fatty-acid oxidation [34]. Therefore, we measured the activity of 3-HAD, a key enzyme in muscle fatty-acid oxidation. The activity was significantly decreased in the HU case compared to that in the control case. CS and MCAD mRNA transcripts levels were significantly decreased in the HU case compared to that in the control case.

To examine whether HU affects the location-specific differences in mitochondrial enzyme activity, an enzyme histochemical SDH staining on cryosections was carried out. SDH activity in SS and IMF regions in the control and hindlimb-unloaded mice was observed (Fig. 3a). The area of SS SDH activity in SDH^{High} myofibers was measured. The SS SDH activity was significantly decreased in the HU case compared to the control case, whereas ratio of SDH activity area to FCSA was insignificantly decreased slightly (Fig. 3b). Furthermore, the length of SS SDH activity in SDH^{High} myofiber was measured. This measurement shows that the length was significantly decreased in the HU case compared to the control case (Fig. 3c). Next, the area of IMF SDH activity in SDH^{High} myofibers was measured. The SDH activity was significantly decreased in the HU case compared to the control case, whereas the ratio of SDH activity area to FCSA was significantly increased (Fig. 3d). In addition, SDH mRNA transcript level was significantly decreased in the HU case compared to the control case (Fig. 3e).

To examine the effects of HU on expression of mitochondrial biogenesis-related genes, RNA samples from the gastrocnemius of control and hindlimb-unloaded mice were subjected to cDNA synthesis and real-time PCR. The PGC-1 family, including PGC-1α, -1β, and PRC, is known to play a central role in mitochondrial biogenesis. PGC-1α mRNA transcript level was significantly increased in the HU case compared to the control case, whereas PGC-1β and PRC mRNA transcript levels were significantly decreased. The transcript level of DNA binding transcription factors, which interact with PGC-1 coregulators, was investigated. Both PPARα and ERRα mRNA transcripts levels were significantly decreased in the HU case compared to the control case. In contrast, NRF-1 mRNA transcript level was insignificantly decreased in the HU case compared to the control case, whereas NRF-2 mRNA transcript level was significantly increased. TFAM and mtSSB function as a key regulator of mammalian mtDNA maintenance. TFAM mRNA transcript level was significantly decreased in the HU case compared to the control

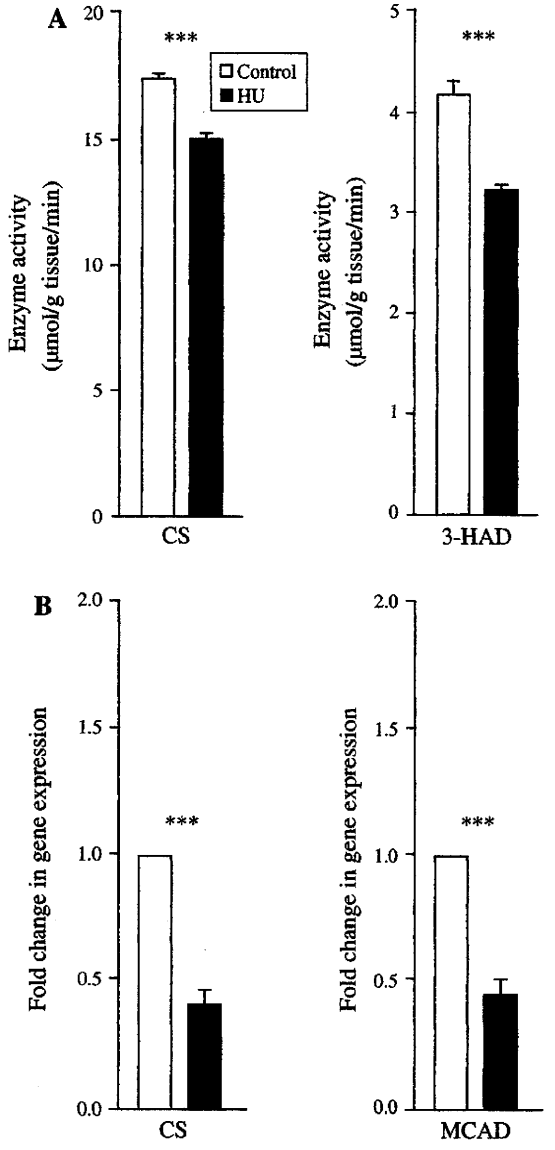

Fig. 3 Effects of HU on activities of mitochondrial enzymes and mRNA expression levels of mitochondrial enzymes. **a** The tissue homogenates were subjected to freeze-thaw cycles, centrifuged, and assayed for enzyme activities. The enzyme activity was normalized for wet weight of skeletal muscle. **b** Total RNA was prepared from muscle tissues and relative gene expression was determined by real-time PCR. The transcript levels were compared to control mice. The data are means ± SEM ($n = 6$). Statistically significant differences compared to control: $^{***}P < 0.001$

case, whereas mtSSB mRNA transcript level was significantly increased (Fig. 4).

The transcript level of two GTPase proteins that act in opposing fusion and fission pathways for maintaining the dynamic of tubular mitochondrial networks were investigated. Both mitofusin 2 mRNA and fission 1 mRNA transcripts levels were significantly decreased in the HU case compared to the control case. ATP-dependent Lon protease mRNA transcript level, which is implicated in mitochondrial protein degradation, was significantly decreased in the HU case compared to the control case (Fig. 5).

Hindlimb unloading increases oxidative stress and disrupts antioxidant capacity in skeletal muscle [35]. MnSOD (localized in the mitochondrial matrix) provides a major defense against oxidative damage by reactive oxygen species (ROS). MnSOD mRNA transcript level remained unchanged in the HU case compared to the control case (Fig. 6).

Discussion

Mammalian mitochondria exhibit a remarkable capacity to adapt to physiological and pathophysiological demands. The processes by which these adaptations occur are thought to be largely achieved at the level of transcriptional regulation. Accordingly, this study focused on the activity of mitochondrial enzymes and the expression of nuclear-encoded genes involved in mitochondrial biogenesis, mitochondrial morphogenesis, and mitochondrial-protein degradation after HU. Our findings provide the insight that mitochondrial adaptations to HU may be associated with distorted gene expression, resulting in changes in the abundance, morphology, and functional properties of mitochondria.

The modified hindlimb suspension model was chosen because it is considered less stressful on the animal than the harness method. Differences in body weights throughout the experimental period can influence interpretation of the experimental results [6]. In our experiment, mice from the hindlimb-unloaded group showed no significant difference in body weight compared with the control group (data not shown), suggesting that the stress effects that occurred during 7 days of HU were minimal. To verify the efficiency of the HU, the changes in myofiber size after 7 days of HU were investigated. The degree of change in our experiment was greater than that in previously reported ones [36, 37]. This difference may be attributed largely to differences between the experimentation set-ups used in the laboratories concerned. The expression of atrogin-1, which is generally recognized as a molecular marker for muscle atrophy, was investigated. A strong up-regulation of atrogin-1 after HU, which is in line with previous reports [38–40], was observed. HU reduced the activity of mitochondrial enzymes as previously reported [9–14]. These findings demonstrate the reliability of our HU model.

Mitochondria that are clustered in proximity to the sarcolemma are termed SS mitochondria, and those embedded among myofibrils are called IMF mitochondria [41]. In this study, SS mitochondria were lost largely than IMF mitochondria after HU. This finding is in keeping with the previous report that the absolute volumes of SS and

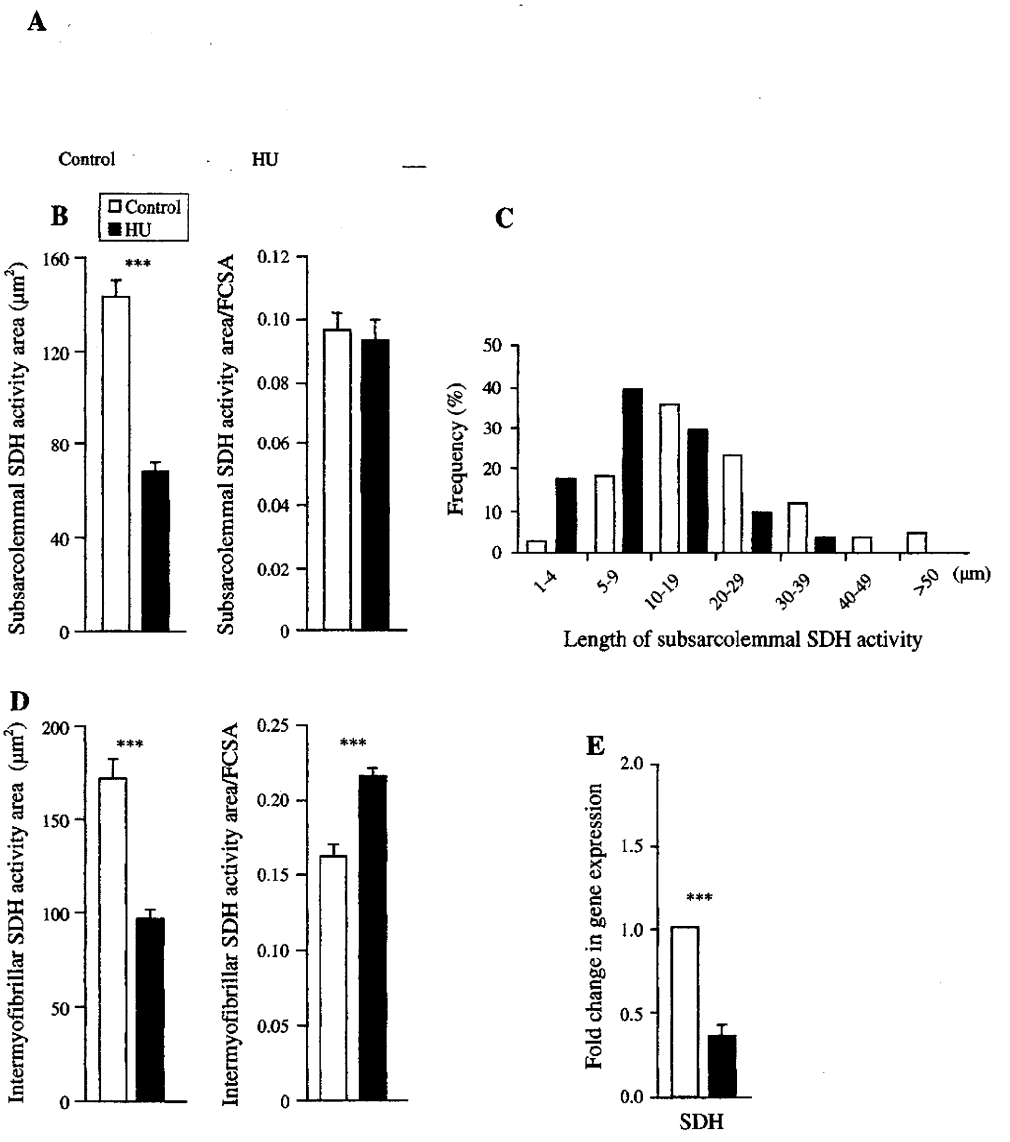

Fig. 4 Regional differences in the mitochondrial adaptations to HU. **a** Histochemical staining for SDH activity was performed on cryosections of the gastrocnemius muscle. *Scale bar* = 50 μm. **b** Quantification of SS SDH staining area in a myofiber was measured with the image-analysis system, calibrated to transform the number of pixels into micrometers. Subsarcolemmal SDH staining area in a myofiber was normalized for FCSA. **c** Quantification of length of SS SDH staining was measured. **d** Quantification of IMF SDH staining area in a myofiber was measured. Intermyofibrillar SDH staining area in a myofiber was normalized for FCSA. **e** Total RNA was prepared from muscle tissues and relative gene expression was determined by real-time PCR. The data are means ± SEM ($n = 6$). Statistically significant differences compared to control: ***$P < 0.001$

IMF mitochondria decrease by 73 and 45% after 5 weeks of hindlimb suspension [42]. We founded that SS mitochondria decreased in proportion to myofiber size but IMF mitochondria increased in proportion to myofiber size, suggesting that SS mitochondria were degraded more rapidly than IMF mitochondria. This phenomenon may be attributable to the development of autophagy. Riley et al. [8] indicated that autolytic degradation occurs during HU in light of the appearance of vacuolation and fragmentation of SS mitochondria.

The possible mechanism for regulating mitochondrial distribution in myofibers is not fully understood. However, it is hypothesized that abnormal distribution of mitochondria during microgravity may be due to disturbance of the structural integrity of mitochondria. In this regard, Nikawa et al. [43] reported that expression of A-kinase anchoring protein and cytoplasmic dynein, which are associated with the anchoring and movement of mitochondria, decreased in spaceflight but not in tail-suspension tests. Indeed, they did not observe abnormal distribution of mitochondria in a tail-suspended rat. This result is inconsistent with previous reports [8, 42] and our present findings. We hypothesized that this phenomenon may be associated with changes in mitochondrial morphology. In this study, therefore, we focused attention on mitochondrial morphogenesis-related genes, namely, mitofusin 2 and fission 1. Consistent with the result presented in a previous report [8], the SS mitochondria (SDH activity) in the HU case were smaller in size than those in the control case (Fig. 7b, c). Moreover, expression of mitofusin 2 decreased after HU. This is a reasonable result because this gene is regulated by PGC-1β and ERRα [44], which are down-regulated by HU. This finding is partially supported by the observation that repression of mitofusin 2 in muscle cells shows a fragmentation of the mitochondrial network [45]. However, we did not observe up-regulation of fission 1, suggesting that

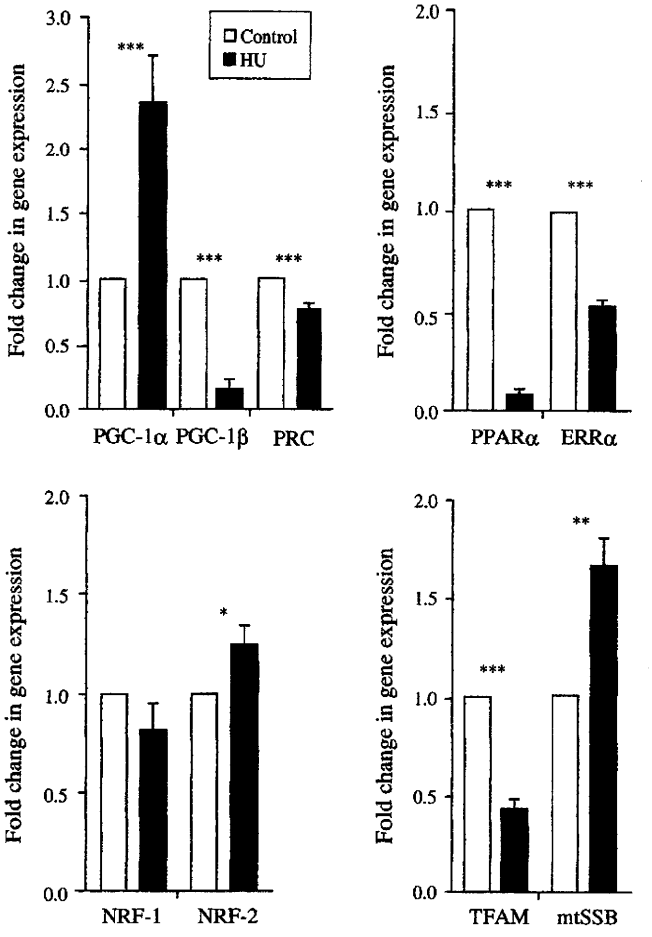

Fig. 5 Effects of HU on expression of mitochondrial biogenesis-related genes. Total RNA was prepared from muscle tissues and relative gene expression was determined by real-time PCR. The transcript levels were compared to control mice. The data are means ± SEM ($n = 6$). Statistically significant differences compared to control: $^{*}P < 0.05$, $^{**}P < 0.01$, and $^{***}P < 0.001$

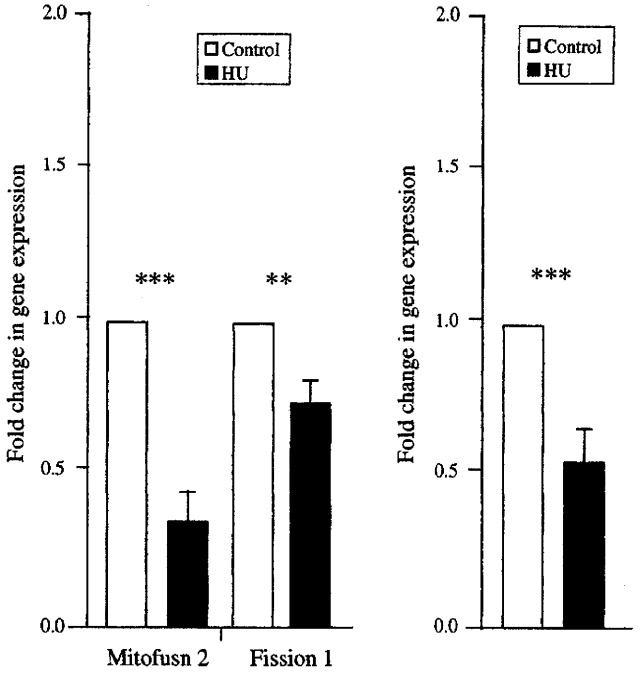

Fig. 6 Effects of HU on expression of mitochondrial morphology and mitochondrial-protein degradation-related genes. Total RNA was prepared from muscle tissues and relative gene expression was determined by real-time PCR. The transcript levels were compared to control mice. The data are means ± SEM ($n = 6$). Statistically significant differences compared to control: $^{**}P < 0.01$ and $^{***}P < 0.001$

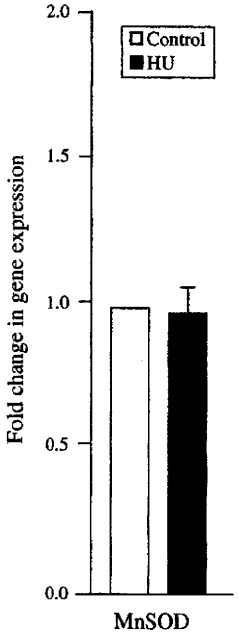

Fig. 7 Effects of HU on mRNA expression levels of mitochondrial antioxidant enzyme. Total RNA was prepared from muscle tissues and relative gene expression was determined by real-time PCR. The transcript levels were compared to control mice. The data are means ± SEM ($n = 6$)

mitochondrial fragmentation induced by HU may be caused by down-regulation of mitofusin 2 irrespective of the expression level of fission 1. However, there is direct evidence that over-expression of fission 1 induces mitochondrial fragmentation of myofibers [46]. This study therefore cannot rule out the possibility that fission 1 may contribute to fragmentation of SS mitochondria during HU. In addition, another mitochondria fission-related gene, dynamin 1-like, may play a role in mitochondrial fragmentation during HU.

Unexpectedly, we observed up-regulation of PGC-1α after HU. This finding is inconsistent with that previously reported by Mazzatti et al. [47] who showed decreased expression of PGC-1α after 24 h of HU. This seemingly contradictory finding implies that the response of PGC-1α may differ in the cases of acute and subacute HU. We attribute this discrepancy to the time course of alterations in electromyographic (EMG) activity during HU. The EMG activity of lateral gastrocnemius decreases by half immediately after HU, stays lower than a control levels for 4–5 days, and subsequently tends to recover by 7 days [48], suggesting that recovery of EMG activity may contribute to augmentation of PGC-1α expression as observed

in this study. There may be several potential intracellular signaling pathways by which PGC-1α gene expression could be regulated during HU. First, calcium signaling pathway may contribute to PGC-1α gene expression because HU promotes Ca^{2+} accumulation in myofibers [49]. Calcium/calmodulin-dependent protein kinase IV likely induces PGC-1α expression by activating cyclic-AMP-responsive-element-binding protein (CREB), which in turn binds to a conserved CRE in the PGC-1α promoter [50]. This pathway is also driven by calcineurin A through myocyte enhancer factor 2, which is a potent *trans*-activator of PGC-1α transcription in skeletal muscle [50]. Interestingly, expression levels of calcineurin mRNA and protein are elevated with HU [51]. Therefore, increased expression of PGC-1α during HU may be explained, at least in part, by activating calcium signaling. Second, HU leads to release of catecholamines [52] that can activate β-adrenergic receptors in skeletal muscle [53]. Activation of these receptors increases intracellular cAMP levels and potentially could activate CREB function on the PGC-1α promoter in skeletal muscle as it does in liver [54]. However, because levels of catecholamine were peaked at 12 h after HU, it is uncertain whether catecholamine-mediated pathway contributes to increased expression of PGC-1α as observed in this study. Third, PGC-1α is also induced via cGMP-dependent signaling resulting from elevated levels of nitric oxide (NO) [55]. It has recently been reported that NO and AMP-activated protein kinase (AMPK) act synergistically to up-regulate PGC-1α mRNA expression in vitro [56]. However, HU decreases expression levels of neuronal nitric oxide synthase protein and mRNA [57] while it increases AMPK activity [58]. Therefore, it remains uncertain as to whether the synergistic effect of NO and AMPK on PGC-1α expression during HU. It is very likely that other signaling cascades also may contribute to PGC-1α expression during HU. Further study would be needed to elucidate the possible mechanisms controlling PGC-1α expression during HU.

It is generally assumed that during HU, expression of genes involved in lipid metabolism is decreased, whereas expression of genes involved in glycolytic enzymes and glycogen synthesis is increased. This hypothesis suggests that switching between lipid usage and carbohydrate usage occurs to meet the metabolic demands of the myofibers during HU. In contrast to PGC-1β and PRC, which were down-regulated by HU, PGC-1α was up-regulated concomitant with decreased expression of its DNA binding transcription factors, PPARα and ERRα, which potently induce fatty-acid oxidation genes, MCAD and carnitine palmitoyltransferase I [59, 60]. Our findings may indicate that PGC-1α does not function harmoniously as a coactivator owing to down-regulation of PPARα and ERRα, leading to reduced expression of fatty-acid metabolism-related genes. This hypothesis may be supported by our results (Fig. 7) and previous articles reports that hindlimb suspension down-regulates gene expression of proteins involved in fatty-acid oxidation [34, 61]. Furthermore, we observed that HU decreased the activity of 3-HAD involved in the β-oxidation of fatty acids. Indeed, Grichko et al. [62] reported that fatty-acid oxidation by isolated mitochondria after 2 weeks of hindlimb suspension is on a declining trend although the difference failed to attain statistical significance. Because our result and previous study [42] show that HU decreases the absolute volumes of mitochondria, we suppose that it may also reduce fatty-acid oxidation of myofibers.

It is well established that TFAM plays a key role in mammalian mtDNA transcription/replication [16], whereas mtSSB contributes to its replication, repair, and recombination [63]. There was no alteration in expression of NRF-1, which is activated by PGC-1α and ERRα but expression of its downstream target gene, TFAM was down-regulated after HU. This down-regulation could contribute to mitochondrial dysfunction by reducing template availability for transcription and translation of key mitochondrial proteins. We observed up-regulation of mtSSB concomitant with moderately increased expression of NRF-2, which is shown to potently activate human mtSSB gene expression [64]. It was shown that mtDNA may accumulate more oxidative DNA damage relative to nuclear DNA [65]. mtSSB up-regulation may therefore be a compensatory response to oxidative stress-induced mtDNA damage during HU.

Lon protease level in skeletal muscle decreases with oxidative stress [66]. Because HU increases oxidative stress [67, 68], our finding may be explained by the oxidative stress induced by HU. This study is, to the best of our knowledge, the first to deal with the potential regulation of Lon protease after HU. It is also possible that down-regulation of Lon protease may be responsible for the accumulation of oxidatively damaged proteins within mitochondria, resulting in impairment of mitochondrial function. For example, aconitase, Kreb's cycle enzyme, is one of many mitochondrial matrix proteins that are preferentially degraded by Lon protease after oxidative modification [69]. In addition to the role of protein degradation, Lon protease can also act as a chaperone independently of its proteolytic activity [19], participate in the regulation of mitochondrial gene expression and genome integrity [70, 71], and regulate apoptotic cell death [19], suggesting that Lon protease may play some role in mitochondrial adaptations to HU. Accordingly, further studies are required to elucidate the role of Lon protease in mitochondrial adaptations to HU.

Besides being the primary site of fuel metabolism and ATP production, mitochondria are also a primary source of ROS. Mitochondria also signal, via ROS and Ca^{2+}, and are

critical regulators of cell death pathways [1]. We measured the expression of MnSOD, a primary mitochondrial antioxidant enzyme involved in quenching ROS concentrations. We hypothesized that if mitochondria of HU mice had a greater antioxidant enzyme activity, this could serve to offset elevated ROS production and reduce ROS-induced damage within mitochondria. However, we found no difference in the expression of MnSOD. This observation is in agreement with previous study reported by Andrianjafiniony et al. [72], who found no change in MnSOD activity after 14 days of HU. This does not preclude the possibility that other antioxidant enzymes may be expressed during HU. Indeed, the activities of copper–zinc superoxide dismutase and catalase are increased in hindlimb-unloaded rat [72]. The lack of adaptation of MnSOD activity to increased oxidative stress by HU suggest that a balance between respiration and ROS generation in mitochondria may be lost, leading to mitochondria-mediated apoptosis. Apoptosis can be evoked by ROS-induced mitochondrial release of the proapoptotic proteins. IMF mitochondria release a great amount of cytochrome c and apoptosis-inducing factor in response to oxidative stress compared with SS mitochondria [73], suggesting that not all mitochondria within a myofiber behave similarly. Given that IMF mitochondria were slowly decreased than SS mitochondria during HU, IMF mitochondria may play a major role in initiating apoptosis.

In conclusion, HU distorts gene expression concerning mitochondrial biogenesis, mitochondrial morphogenesis, and mitochondrial-protein degradation, resulting in changes in the abundance, morphology, and functional properties of mitochondria. Unexpectedly, PGC-1α expression is up-regulated after HU. It is unlikely that the augmentation would contribute to mitochondrial biogenesis, because several genes controlled by PGC-1α are down-regulated, suggesting that coordinated expression of PGC-1 family coactivators and DNA binding transcription factors is required for maintaining mitochondrial biogenesis in skeletal muscle. Furthermore, down-regulation of mitochondrial morphology-related genes associated with HU may be also involved in alterations in intracellular mitochondrial distribution. Our findings provide insight into the mitochondrial adaptation in skeletal muscle to HU. Interestingly, Romanello et al. [46] suggest that mitochondrial remodeling contributes to muscle atrophy. Mitochondrial adaptations may therefore have to be considered as an important event when interpreting the results of HU experiments.

Acknowledgments This research was supported by the MEXT (The Ministry of Education, Culture, Sports, Science and Technology) (Grant-in Aid for Scientific Research (C), 22500658), Japan. This research was also partially supported by grants 18A-1 for Nervous and Mental Disorders and H19-kokoro-020 for Research in Brain Science from MHLW (The Ministry of Health, Labour and Welfare), Japan.

References

1. Hock MB, Kralli A (2009) Transcriptional control of mitochondrial biogenesis and function. Annu Rev Physiol 71:177–203
2. Hood DA (2001) Invited review: contractile activity-induced mitochondrial biogenesis in skeletal muscle. J Appl Physiol 90:1137–1157
3. Booth FW (1982) Effect of limb immobilization on skeletal muscle. J Appl Physiol 52:1113–1118
4. Thomason DB, Booth FW (1990) Atrophy of the soleus muscle by hindlimb unweighting. J Appl Physiol 68:1–12
5. Wicks KL, Hood DA (1991) Mitochondrial adaptations in denervated muscle: relationship to muscle performance. Am J Physiol 260:C841–C850
6. Morey-Holton ER, Globus RK (2002) Hindlimb unloading rodent model: technical aspects. J Appl Physiol 92:1367–1377
7. Talmadge RJ (2000) Myosin heavy chain isoform expression following reduced neuromuscular activity: potential regulatory mechanisms. Muscle Nerve 23:661–679
8. Riley DA, Slocum GR, Bain JL, Sedlak FR, Sowa TE, Mellender JW (1990) Rat hindlimb unloading: soleus histochemistry, ultrastructure, and electromyography. J Appl Physiol 69:58–66
9. Yajid F, Mercier JG, Mercier BM, Dubouchaud H, Préfaut C (1998) Effects of 4 wk of hindlimb suspension on skeletal muscle mitochondrial respiration in rats. J Appl Physiol 84:479–485
10. Desplanches D, Mayet MH, Sempore B, Flandrois R (1987) Structural and functional responses to prolonged hindlimb suspension in rat muscle. J Appl Physiol 63:558–563
11. Roy RR, Bello MA, Bouissou P, Edgerton VR (1987) Size and metabolic properties of fibers in rat fast-twitch muscles after hindlimb suspension. J Appl Physiol 62:2348–2357
12. Fell RD, Steffen JM, Musacchia XJ (1985) Effect of hypokinesia-hypodynamia on rat muscle oxidative capacity and glucose uptake. Am J Physiol 249:R308–R312
13. Flynn DE, Max SR (1985) Effects of suspension hypokinesia/hypodynamia on rat skeletal muscle. Aviat Space Environ Med 56:1065–1069
14. Simard C, Lacaille M, Vallières J (1985) Enzymatic adaptations to suspension hypokinesia in skeletal muscle of young and old rats. Mech Ageing Dev 33:1–9
15. Ryan MT, Hoogenraad NJ (2007) Mitochondrial-nuclear communications. Annu Rev Biochem 76:701–722
16. Scarpulla RC (2008) Transcriptional paradigms in mammalian mitochondrial biogenesis and function. Physiol Rev 88:611–638
17. Chen H, Chan DC (2005) Emerging functions of mammalian mitochondrial fusion and fission. Hum Mol Genet 14:R283–R289
18. Ventura-Clapier R, Garnier A, Veksler V (2008) Transcriptional control of mitochondrial biogenesis: the central role of PGC-1alpha. Cardiovasc Res 79:208–217
19. Bota DA, Ngo JK, Davies KJ (2005) Downregulation of the human Lon protease impairs mitochondrial structure and function and causes cell death. Free Radic Biol Med 38:665–677
20. Krieger DA, Tate CA, McMillin-Wood J, Booth FW (1980) Populations of rat skeletal muscle mitochondria after exercise and immobilization. J Appl Physiol 48:23–28
21. Moley-Holtone E, Wronski TJ (1981) Animal models for stimulating weightlessness. Physiologist 24:S45–S48
22. McCarthy JJ, Fox AM, Tsika GL, Gao L, Tsika RW (1997) beta-MHC transgene expression in suspended and mechanically

overloaded/suspended soleus muscle of transgenic mice. Am J Physiol 272:R1552–R1561
23. Srere PA (1969) Citrate synthase. Methods Enzymol 13:3–5
24. Bass A, Brdiczka D, Eyer P, Hofer S, Pette D (1969) Metabolic differentiation of distinct muscle types at the level of enzymatic organization. Eur J Biochem 10:198–206
25. Nachlas MM, Tsou KC, DeSousa E, Cheng CS, Seligman AM (1957) Cytochemical demonstration of succinic dehydrogenase by the use of the new p-nitrophenyl substituted ditetrazole. J Histochem Cytochem 5:420–436
26. van den Bosch BJ, van den Burg CM, Schoonderwoerd K, Lindsey PJ, Scholte HR, de Coo RF, van Rooij E, Rockman HA, Doevendans PA, Smeets HJ (2005) Regional absence of mitochondria causing energy depletion in the myocardium of muscle LIM protein knockout mice. Cardiovasc Res 65:411–418
27. Fischer M, You M, Matsumoto M, Crabb DW (2003) Peroxisome proliferator-activated receptor alpha (PPARalpha) agonist treatment reverses PPARalpha dysfunction and abnormalities in hepatic lipid metabolism in ethanol-fed mice. J Biol Chem 278: 27997–28004
28. Wiwi CA, Gupte M, Waxman DJ (2004) Sexually dimorphic P450 gene expression in liver-specific hepatocyte nuclear factor 4alpha-deficient mice. Mol Endocrinol 18:1975–1987
29. Kraft CS, LeMoine CM, Lyons CN, Michaud D, Mueller CR, Moyes CD (2006) Control of mitochondrial biogenesis during myogenesis. Am J Physiol 290:C1119–C1127
30. Masuyama M, Iida R, Takatsuka H, Yasuda T, Matsuki T (2005) Quantitative change in mitochondrial DNA content in various mouse tissues during aging. Biochim Biophys Acta 1723:302–308
31. Suliman HB, Carraway MS, Welty-Wolf KE, Whorton AR, Piantadosi CA (2003) Lipopolysaccharide stimulates mitochondrial biogenesis via activation of nuclear respiratory factor-1. J Biol Chem 278:41510–41518
32. Schreiber SN, Knutti D, Brogli K, Uhlmann T, Kralli A (2003) The transcriptional coactivator PGC-1 regulates the expression and activity of the orphan nuclear receptor estrogen-related receptor alpha (ERRalpha). J Biol Chem 278:9013–9018
33. Guo Z, Boekhoudt GH, Boss JM (2003) Role of the intronic enhancer in tumor necrosis factor-mediated induction of manganous superoxide dismutase. J Biol Chem 278:23570–23578
34. Stein T, Schluter M, Galante A, Soteropoulos P, Tolias P, Grindeland R, Moran M, Wang T, Polansky M, Wade C (2002) Energy metabolism pathways in rat muscle under conditions of simulated microgravity. J Nutr Biochem 13:471–478
35. Lawler JM, Song W, Demaree SR (2003) Hindlimb unloading increases oxidative stress and disrupts antioxidant capacity in skeletal muscle. Free Radic Biol Med 35:9–16
36. Carlson CJ, Booth FW, Gordon SE (1999) Skeletal muscle myostatin mRNA expression is fiber-type specific and increases during hindlimb unloading. Am J Physiol 277:R601–R606
37. Stelzer JE, Widrick JJ (2003) Effect of hindlimb suspension on the functional properties of slow and fast soleus fibers from three strains of mice. J Appl Physiol 95:2425–2433
38. Stevenson EJ, Giresi PG, Koncarevic A, Kandarian SC (2003) Global analysis of gene expression patterns during disuse atrophy in rat skeletal muscle. J Physiol 551:33–48
39. Bodine SC, Latres E, Baumhueter S, Lai VK, Nunez L, Clarke BA, Poueymirou WT, Panaro FJ, Na E, Dharmarajan K, Pan ZQ, Valenzuela DM, DeChiara TM, Stitt TN, Yancopoulos GD, Glass DJ (2001) Identification of ubiquitin ligases required for skeletal muscle atrophy. Science 294:1704–1708
40. Gomes MD, Lecker SH, Jagoe RT, Navon A, Goldberg AL (2001) Atrogin-1, a muscle-specific F-box protein highly expressed during muscle atrophy. Proc Natl Acad Sci 98:14440–14445
41. Hoppeler H (1986) Exercise-induced ultrastructural changes in skeletal muscle. Int J Sports Med 7:187–204
42. Desplanches D, Kayar SR, Sempore B, Flandrois R, Hoppeler H (1990) Rat soleus muscle ultrastructure after hindlimb suspension. J Appl Physiol 69:504–508
43. Nikawa T, Ishidoh K, Hirasaka K, Ishihara I, Ikemoto M, Kano M, Kominami E, Nonaka I, Ogawa T, Adams GR, Baldwin KM, Yasui N, Kishi K, Takeda S (2004) Skeletal muscle gene expression in space-flown rats. FASEB J 18:522–524
44. Liesa M, Borda-d'Agua B, Medina-Gómez G, Lelliott CJ, Paz JC, Rojo M, Palacín M, Vidal-Puig A, Zorzano A (2008) Mitochondrial fusion is increased by the nuclear coactivator PGC-1beta. PLoS ONE 3:e3613
45. Pich S, Bach D, Briones P, Liesa M, Camps M, Testar X, Palacín M, Zorzano A (2005) The Charcot-Marie-Tooth type 2A gene product, Mfn2, up-regulates fuel oxidation through expression of OXPHOS system. Hum Mol Genet 14:1405–1415
46. Romanello V, Guadagnin E, Gomes L, Roder I, Sandri C, Petersen Y, Milan G, Masiero E, Del Piccolo P, Foretz M, Scorrano L, Rudolf R, Sandri M (2010) Mitochondrial fission and remodelling contributes to muscle atrophy. EMBO J 29:1774–1785
47. Mazzatti DJ, Smith MA, Oita RC, Lim FL, White AJ, Reid MB (2008) Muscle unloading-induced metabolic remodeling is associated with acute alterations in PPARdelta and UCP-3 expression. Physiol Genomics 34:149–161
48. Alford EK, Roy RR, Hodgson JA, Edgerton VR (1987) Electromyography of rat soleus, medial gastrocnemius, and tibialis anterior during hind limb suspension. Exp Neurol 96:635–649
49. Ingalls CP, Warren GL, Armstrong RB (1999) Intracellular Ca2+ transients in mouse soleus muscle after hindlimb unloading and reloading. J Appl Physiol 87:386–390
50. Handschin C, Rhee J, Lin J, Tarr PT, Spiegelman BM (2003) An autoregulatory loop controls peroxisome proliferator-activated receptor gamma coactivator 1alpha expression in muscle. Proc Natl Acad Sci 100:7111–7116
51. Dupont-Versteegden EE, Knox M, Gurley CM, Houlé JD, Peterson CA (2002) Maintenance of muscle mass is not dependent on the calcineurin-NFAT pathway. Am J Physiol 282:C1387–C1395
52. Aviles H, Belay T, Vance M, Sonnenfeld G (2005) Effects of space flight conditions on the function of the immune system and catecholamine production simulated in a rodent model of hindlimb unloading. Neuroimmunomodulation 12:173–181
53. Sakamoto K, Goodyear LJ (2002) Invited review: intracellular signaling in contracting skeletal muscle. J Appl Physiol 93: 369–383
54. Herzig S, Long F, Jhala US, Hedrick S, Quinn R, Bauer A, Rudolph D, Schutz G, Yoon C, Puigserver P, Spiegelman B, Montminy M (2001) CREB regulates hepatic gluconeogenesis through the coactivator PGC-1. Nature 413:179–183
55. Nisoli E, Clementi E, Paolucci C, Cozzi V, Tonello C, Sciorati C, Bracale R, Valerio A, Francolini M, Moncada S, Carruba MO (2003) Mitochondrial biogenesis in mammals: the role of endogenous nitric oxide. Science 299:896–899
56. Lira VA, Brown DL, Lira AK, Kavazis AN, Soltow QA, Zeanah EH, Criswell DS (2010) Nitric oxide and AMPK cooperatively regulate PGC-1 in skeletal muscle cells. J Physiol 588: 3551–3566
57. Tidball JG, Lavergne E, Lau KS, Spencer MJ, Stull JT, Wehling M (1998) Mechanical loading regulates NOS expression and activity in developing and adult skeletal muscle. Am J Physiol 275:C260–C266
58. Hilder TL, Baer LA, Fuller PM, Fuller CA, Grindeland RE, Wade CE, Graves LM (2005) Insulin-independent pathways mediating glucose uptake in hindlimb-suspended skeletal muscle. J Appl Physiol 99:2181–2188
59. Sladek R, Bader JA, Giguère V (1997) The orphan nuclear receptor estrogen-related receptor alpha is a transcriptional

regulator of the human medium-chain acyl coenzyme A dehydrogenase gene. Mol Cell Biol 17:5400–5409
60. Vega RB, Huss JM, Kelly DP (2000) The coactivator PGC-1 cooperates with peroxisome proliferator-activated receptor alpha in transcriptional control of nuclear genes encoding mitochondrial fatty acid oxidation enzymes. Mol Cell Biol 20:1868–1876
61. Wittwer M, Fluck M, Hoppeler H, Muller S, Desplanches D, Billeter R (2002) Prolonged unloading of rat soleus muscle causes distinct adaptations of the gene profile. FASEB J 6: 884–886
62. Grichko VP, Heywood-Cooksey A, Kidd KR, Fitts RH (2000) Substrate profile in rat soleus muscle fibers after hindlimb unloading and fatigue. J Appl Physiol 88:473–478
63. Tomáska L, Nosek J, Kucejová B (2001) Mitochondrial single-stranded DNA-binding proteins: in search for new functions. Biol Chem 382:179–186
64. Bruni F, Polosa PL, Gadaleta MN, Cantatore P, Roberti M (2010) Nuclear respiratory factor 2 induces the expression of many but not all human proteins acting in mitochondrial DNA transcription and replication. J Biol Chem 285:3939–3948
65. Yakes FM, Van Houten B (1997) Mitochondrial DNA damage is more extensive and persists longer than nuclear DNA damage in human cells following oxidative stress. Proc Natl Acad Sci 94:514–519
66. Bota DA, Van Remmen H, Davies KJ (2002) Modulation of Lon protease activity and aconitase turnover during aging and oxidative stress. FEBS Lett 532:103–106
67. Siu PM, Pistilli EE, Alway SE (2008) Age-dependent increase in oxidative stress in gastrocnemius muscle with unloading. J Appl Physiol 105:1695–1705
68. Servais S, Letexier D, Favier R, Duchamp C, Desplanches D (2007) Prevention of unloading-induced atrophy by vitamin E supplementation: links between oxidative stress and soleus muscle proteolysis? Free Radic Biol Med 42:627–635
69. Bota DA, Davies KJ (2002) Lon protease preferentially degrades oxidized mitochondrial aconitase by an ATP-stimulated mechanism. Nat Cell Biol 4:674–680
70. Fu GK, Markovitz DM (1998) The human LON protease binds to mitochondrial promoters in a single-stranded, site-specific, strand-specific manner. Biochemistry 37:1905–1909
71. Langer T, Neupert W (1996) Regulated protein degradation in mitochondria. Experientia 52:1069–1076
72. Andrianjafiniony T, Dupré-Aucouturier S, Letexier D, Couchoux H, Desplanches D (2010) Oxidative stress, apoptosis, and proteolysis in skeletal muscle repair after unloading. Am J Physiol 299:C307–C315
73. Adhihetty PJ, Ljubicic V, Menzies KJ, Hood DA (2005) Differential susceptibility of subsarcolemmal and intermyofibrillar mitochondria to apoptotic stimuli. Am J Physiol 289:C994–C1001

Neuroscience Research 70 (2011) 189–196

Contents lists available at ScienceDirect

Neuroscience Research

journal homepage: www.elsevier.com/locate/neures

Relationship of negative mood with prefrontal cortex activity during working memory tasks: An optical topography study

Ryuta Aoki[a,b,*], Hiroki Sato[c,**], Takusige Katura[c], Kei Utsugi[d], Hideaki Koizumi[c], Ryoichi Matsuda[a], Atsushi Maki[c]

[a] Department of Life Sciences, Graduate School of Arts and Sciences, The University of Tokyo, 3-8-1 Komaba, Meguro-ku, Tokyo 153-8902, Japan
[b] Japan Society for the Promotion of Science, 8 Ichibancho, Chiyoda-ku, Tokyo 102-8472, Japan
[c] Advanced Research Laboratory, Hitachi, Ltd., 2520 Akanuma, Hatoyama, Saitama, 350-0395, Japan
[d] Systems Development Laboratory, Hitachi, Ltd., 292 Yoshida-cho, Totsuka-ku, Yokohama, Kanagawa 244-0817, Japan

ARTICLE INFO

Article history:
Received 15 December 2010
Received in revised form 24 February 2011
Accepted 25 February 2011
Available online 5 March 2011

Keywords:
Emotion–cognition interaction
Prefrontal cortex
Near-infrared spectroscopy (NIRS)
Optical topography
Profile of Mood States (POMS)

ABSTRACT

Mood has a substantial impact on cognitive functions. Although studies have shown that the interaction between mood and cognition is mediated by the prefrontal cortex (PFC), little is known about how naturalistic mood in everyday life is associated with PFC activity during cognitive tasks. We investigated whether inter-individual variation in perceived mood under current life situations (recent week) is related to PFC activity during working memory (WM) tasks in healthy adults. Levels of positive and negative moods were quantified with the Profile of Mood States (POMS) questionnaire. PFC activities during verbal and spatial WM tasks were measured by optical topography (OT), a non-invasive low-constraint neuroimaging tool, to minimize experimental intervention in participants' moods. Group-average analysis showed significant activations in the bilateral dorsolateral PFC in both WM tasks. Correlation analysis revealed that the participants reporting higher levels of negative moods showed lower levels of PFC activity during the verbal WM task but not during the spatial WM task. This relationship was significant even after controlling for possible confounding factors such as age, gender, and task performance. Our results suggest that verbal WM is linked with naturalistic negative mood and that the PFC is involved in the mood–cognition interaction in daily circumstances.

1. Introduction

In everyday life, the way we think and act is substantially affected by our mood, regardless of whether we recognize it or not. Psychologists have long investigated the relationship between mood and cognition, revealing that many cognitive functions are actually modulated by mood (Mitchell and Phillips, 2007; Robinson and Sahakian, 2009). An important cognitive function in the mood-cognition interaction is working memory (WM), a mental process well documented in both psychology and neuroscience (Baddeley, 2003). Behavioral studies have shown that performance on various cognitive tasks requiring WM (e.g., word span task, Tower of London planning task) is affected by the participant's mood Mitchell and Phillips (2007). Psychopharmacological studies and theoretical models have also suggested that mood and relevant neurotransmitters (e.g., dopamine and serotonin) are linked with WM performance (Ashby et al., 1999; Luciana et al., 1998).

Neuroimaging research has begun to elucidate the underlying neural mechanisms of the mood-cognition interaction in WM. As the prefrontal cortex (PFC) has been demonstrated to play a crucial role in WM (Smith and Jonides, 1999; Smith et al., 1996), the effect of mood on WM is likely mediated by the PFC function. Indeed, a functional magnetic resonance imaging (fMRI) study showed that activity in the dorsolateral PFC (DLPFC) during a WM task (numerical N-back task) was reduced when the participants were exposed to acute psychological stress (induced by viewing aversive movie clips), which led to increased negative mood (Qin et al., 2009). This finding is consistent with the results of other fMRI studies showing that WM-related activity in the DLPFC is attenuated by affective modulation using negative emotional stimuli (Anticevic et al., 2010; Perlstein et al., 2002). These results provide valuable insight into the role of the PFC in the interaction between mood and WM.

However, experimentally induced mood may be different from naturalistic mood in its relationship with cognition. Characteristics of induced moods (e.g., intensity, duration, and whether

* Corresponding author. Tel.: +81 3 5454 6637; fax: +81 3 5454 4306.
** Co-corresponding author. Tel.: +81 49 296 6111; fax: +81 49 296 5999.
E-mail addresses: cc097702@mail.ecc.u-tokyo.ac.jp, ryuta.aoki.mu@hitachi.com (R. Aoki), hiroki.sato.ry@hitachi.com (H. Sato).

0168-0102/$ – see front matter © 2011 Elsevier Ireland Ltd and the Japan Neuroscience Society. All rights reserved.
doi:10.1016/j.neures.2011.02.011

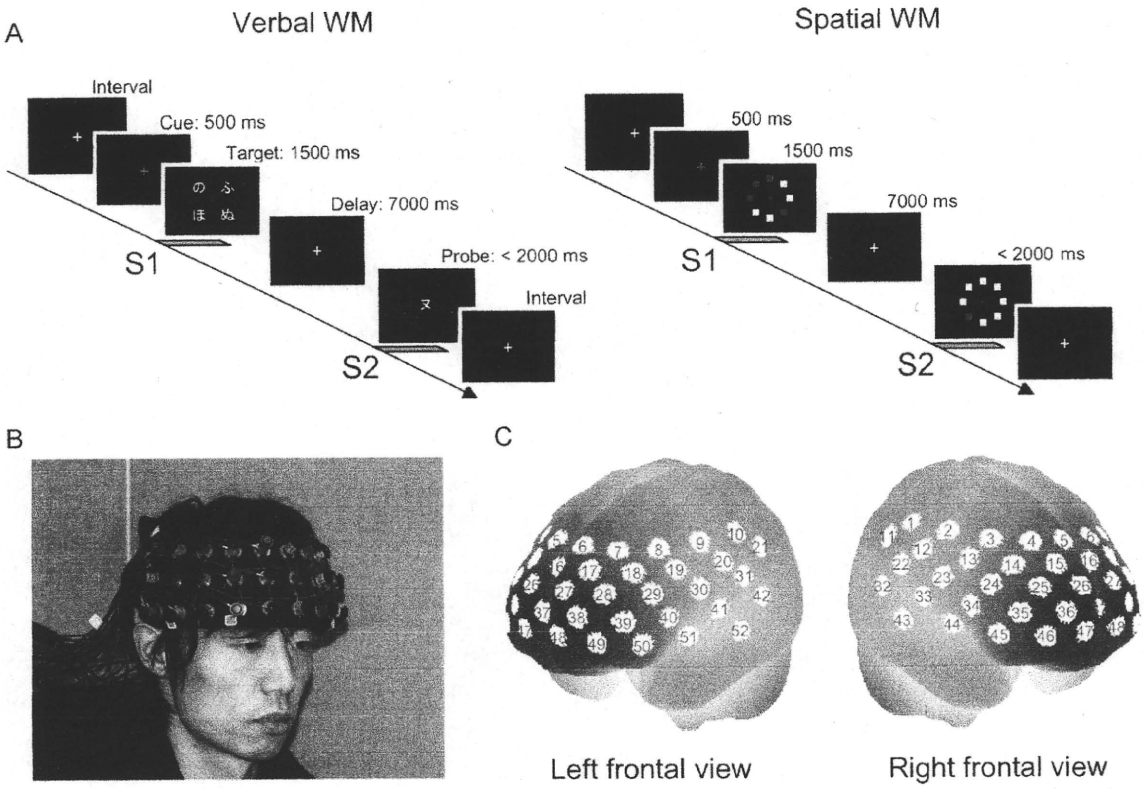

Fig. 1. Task paradigm and experimental setting. (A) Schematic diagrams of verbal and spatial WM tasks. Participants were instructed to remember the target stimuli (S1) and to report whether the character (verbal WM task) or location of a red square (spatial WM task) presented in the probe stimuli (S2) was identical to one of the items in S1. (B) OT probe-holder worn by participant. A 3 × 11 probe array (17 light sources and 16 detectors) was positioned on the forehead. (C) Arrangement of measurement positions (52 channels) in MNI space, which was estimated by means of probabilistic registration method (Singh et al., 2005).

the demand effect exists) depend on various methods of mood induction procedures (Martin, 1990) and may differ qualitatively from those of naturalistic moods. Indeed, a previous study demonstrated that induced moods and naturalistic moods can occasionally exert different, or even opposite, effects on certain aspects of cognitive functions (Parrot and Sabini, 1990). To understand the mood-cognition interaction more thoroughly, evidence from both induced and naturalistic moods should be converged (Mayer et al., 1995). Thus, the relationship between naturalistic mood and WM is worth investigating in neuroimaging studies, in addition to previous research using affective modulation paradigms.

In this study, we investigated whether and how naturalistic moods in healthy adults are associated with PFC activity during WM tasks. We used individual differences (Kosslyn et al., 2002), which enable exploring the relationship between mood and brain activity without any explicit mood induction. Specifically, we tested whether inter-individual variations in the levels of positive or negative moods are correlated with PFC activity in response to the WM tasks. Participants' naturalistic moods in their current life (the last week) were assessed with the Profile of Mood States (McNair et al., 1971; Yokoyama et al., 1990), a self-report questionnaire used in previous studies that examined the PFC role in the mood-cognition interaction (Canli et al., 2004; Harrison et al., 2009). PFC activity during WM tasks was measured with optical topography (OT), a non-invasive, low-constraint neuroimaging technique, to minimize the mood modulation due to the experiment. OT enables measuring hemodynamic responses in the cerebral cortex under near-natural situations (e.g., sitting position) (Maki et al., 1995; Tsujimoto et al., 2004) and can tap into relationships between naturalistic mood and PFC activity (Suda et al., 2009; Suda et al., 2008). We used two types of WM tasks (verbal and spatial) that had an identical delayed-response paradigm, a standard cognitive activation paradigm often used in the human neuroimaging studies of WM (Smith and Jonides, 1999; Smith et al., 1996).

2. Materials and methods

2.1. Participants

Thirty-two healthy adults participated in the experiment after they provided written informed consent. Their handedness was assessed with the Edinburgh Handedness Inventory (Oldfield, 1971), and data from a female who demonstrated left-handedness were excluded from the analysis. Data from two other females were also excluded from the analysis because of their poor behavioral performance (<50% correct responses for the spatial WM tasks). The remaining 29 participants (12 females, 17 males, mean age = 35.9 years, SD = 7.7, and range = 25–58, all right handed) were included in the final analysis. The study was approved by the Ethics Committee of Hitachi, Ltd.

2.2. Mood assessment

The participants' naturalistic moods were assessed by means of a short form of the Profile of Mood States (McNair et al., 1971), which has been translated and validated for the Japanese general population (Yokoyama et al., 1990). McNair et al. (1971) defined moods as mild, pervasive, and generalized affective states that are perceived subjectively by individuals. The participants rated 30 mood-related adjectives on a 5-point scale ranging from 0 ("not at all") to 4 ("extremely") on the basis of how they had been feeling during the past week. While the POMS consists of six identifiable mood factors (tension, depression, anger, vigor, fatigue, and confusion), our study focused on the POMS positive mood score (the score of vigor subscale) and the POMS negative mood score (the sum of the score for the other five subscales), following a previous study (Canli et al., 2004).

2.3. WM tasks

The tasks were presented through software, the Platform of Stimuli and Tasks (developed by Hitachi, ARL). Each participant performed two types of WM tasks (verbal and spatial), which had an identical delayed-response paradigm (Fig. 1A). In both tasks, each trial started with a 1500-ms presentation of the target stimuli (S1), which was followed by a delay of 7000 ms. A probe stimulus (S2) was then presented for 2000 ms or until the participant responded. The intervals between S2 onset and the following S1 onset in the next trial were randomized from 16 to 24 s. Only a